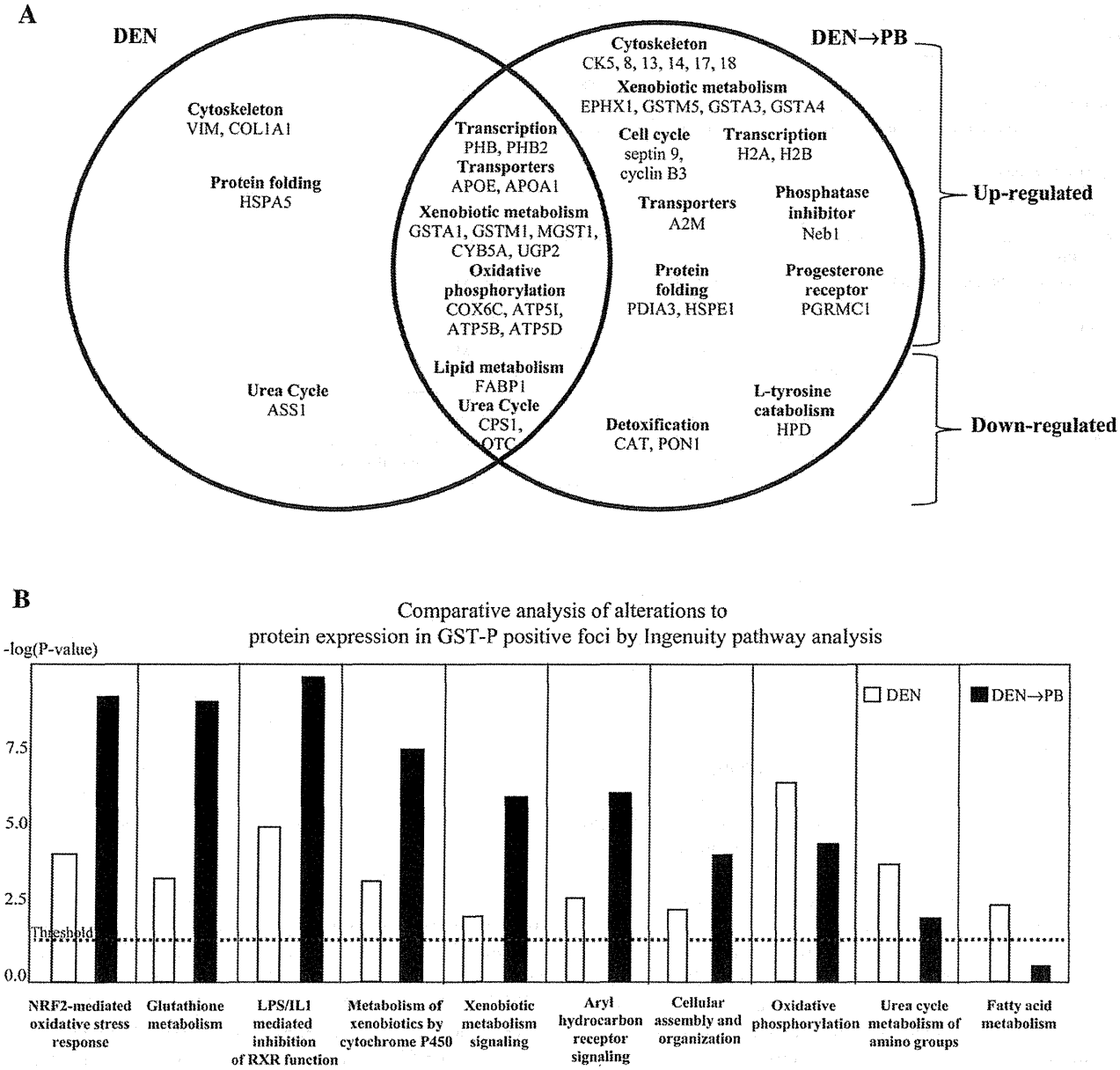

FIG. 1. Ingenuity pathway analysis for alterations to protein expression in liver GST-P$^+$ foci of rats treated with DEN followed by PB at a dose of 0 and 500 ppm for 10 weeks. (A) A Venn diagram comparing alterations to protein expression in GST-P$^+$ foci of rats treated with DEN alone and DEN followed by PB. (B) Comparative analysis of changes to canonical pathways in the GST-P$^+$ foci of rats in initiation control and promotion groups 13 weeks after DEN initiation. Numbers of proteins with altered expression are represented as (−log(*p* value)).

et al., 2010). It was further reported that an aberrant continuous activation of NRF2 in premalignant cells can promote cancer cell survival in response to an oxidizing tumor environment, which can be encountered by activation of oncogenic signals, altered metabolism, and mitochondrial dysfunction. Moreover, an important facet of NRF2 function is that it can cross-regulate the expression of factors controlling other signaling pathways, including the AhR and the NF-κB pathway (Kensler and Wakabayashi, 2010). On the other hand, AhR is known to interact with signaling pathways that are mediated by estrogen receptor and other hormone receptors, hypoxia, NF-κB, and to transactivate c-*myc* gene (Carlson and Perdew, 2002). Newly detected elevation of PHB and PHB2 in GST-P$^+$ foci as well as HCCs suggested the important role of these two proteins in onset of hepatocarcinogenesis. In line with our results, proteome analysis of the human HCC cell line, HCC-M,

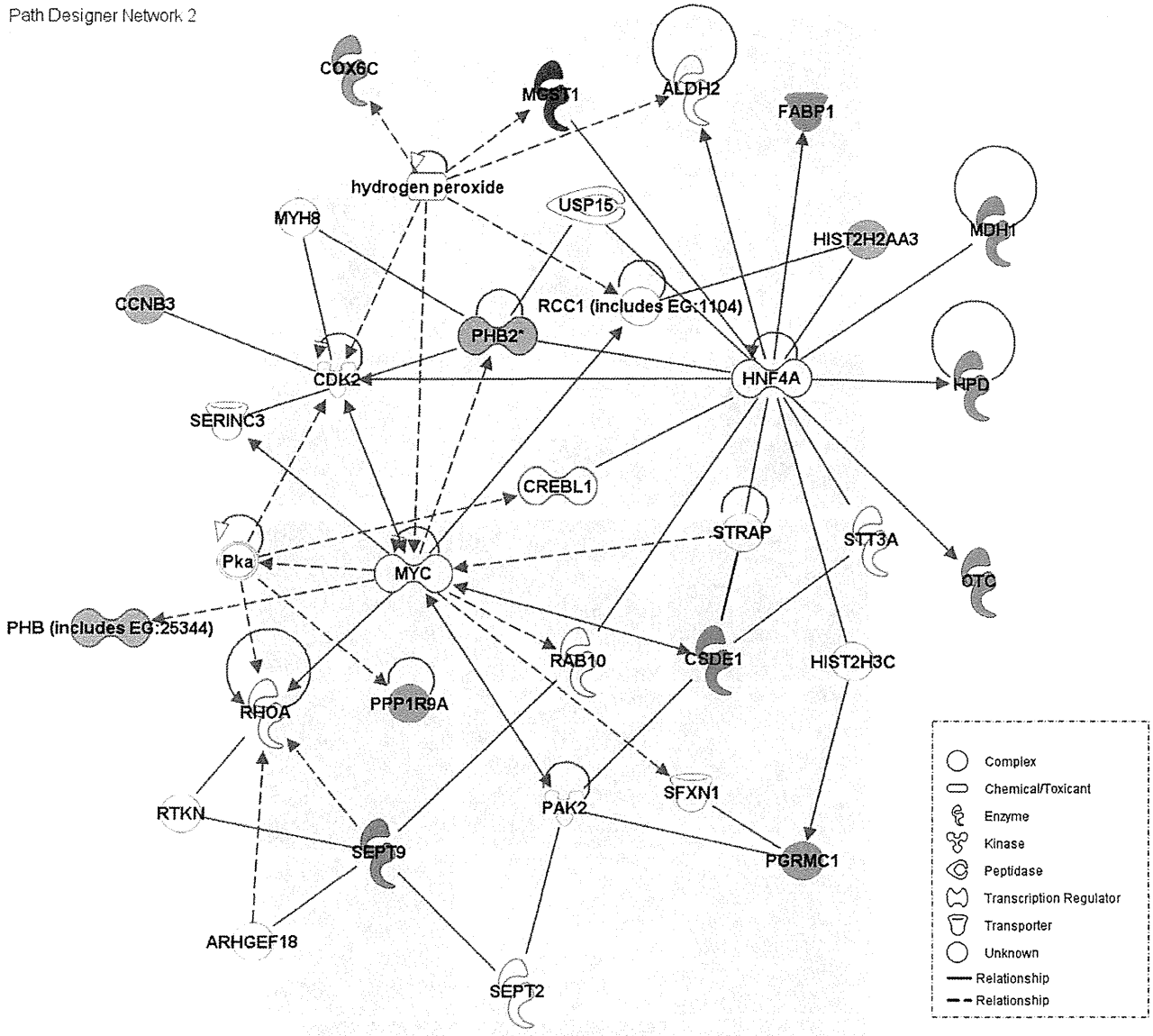

FIG. 2. Signaling pathway involving differentially expressed proteins in GST-P$^+$ foci of rats treated with DEN followed by PB at a dose 500 ppm controlled by c-myc and HNF-4 transcriptional factors. Note overexpression (red) of PHB, PHB2, SEPT9, Neb1 (PPP1R9A), PGRMC1, histone H2aa3 (HIST2H2AA3) and downregulation (green) of OTC, HPD, and FAPB1.

revealed elevation of PHB (Seow *et al.*, 2000). It has been demonstrated that two PHB proteins, Phb1p and Phb2p, are located in the mitochondrial inner membrane where they form a large complex that represents a novel type of membrane-bound chaperone (Nijtmans *et al.*, 2002). The PHB complex binds directly to newly synthesized mitochondrial translation products and stabilizes them against degradation by membrane-bound metalloproteases belonging to the family of mitochondrial triple-A proteins. Human prohibitins have also been suggested to be localized in the nucleus and modulate transcriptional activity by interacting with various transcription factors, including nuclear receptors, either directly or indirectly (Tatsuta *et al.*, 2005). Recently, they have been demonstrated to be positive, rather than negative, regulators of cell proliferation in both plants and mice (Merkwirth *et al.*, 2008). Furthermore, PHB has been shown to colocalize with Rb in the nucleus, participating in transcriptional repression via N-CoR and HDAC1, inducing G1/S cell cycle arrest and associating with p53, thus, inhibiting apoptosis (Fusaro *et al.*, 2002). It has been further reported to interact with RING finger protein 2 (RNF2), a member of the PcG (polycomb group) family of proteins, and that the two proteins regulate the

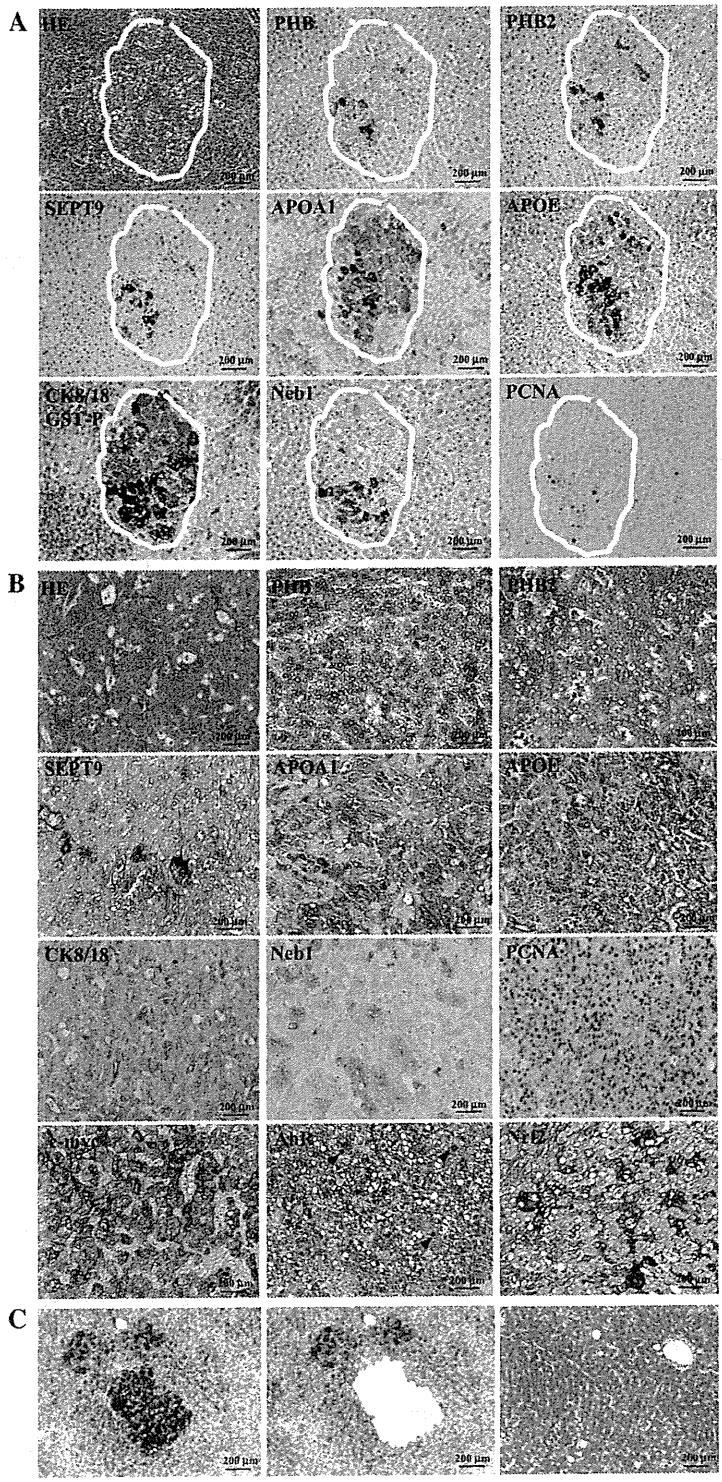

FIG. 3. Immunohistochemical analysis of PHB, PHB2, SEPT9, Neb1, CK8/18, APOE, APOA1, PCNA, c-myc, NRF2, and AhR in serial sections of rat livers after DEN initiation followed by PB at a dose of 500 ppm. GST-P (red) and CK8/18 (brown) positivity was demonstrated by double immunohistochemistry. (A) IHC analysis of protein expression in GST-P$^+$ foci of rats initiated with DEN followed by PB for 10 weeks. Note the coordinated staining pattern of overexpressed proteins in GST-P$^+$ foci. (B) IHC analysis of protein expression in HCCs of rats initiated with DEN followed by PB for 33 weeks. Arrows, overexpression of NRF2 and AhR in the nuclei of tumor cells in HCC. (C) Microdissected GST-P$^+$ foci and the photograph of the normal-appearing liver tissue of the rat initiated with DEN followed by PB for 10 weeks.

activity of E2F1 transcriptional factor via dual pathways: the direct, prohibitin-mediated pathway and the indirect, p16-mediated pathway of E2F1 transcriptional regulation (Choi *et al.*, 2008). PHB overexpression was shown to increase the expression of GST-P in intestinal cells and protect against oxidant-induced depletion of glutathione (Theiss *et al.*, 2007). In other studies, a striking correlation was revealed between mitochondrial targeting and the maintenance of cell proliferation, pointing to a crucial role of PHB2 within mitochondria (Tatsuta *et al.*, 2005). PHB2 is involved in recruitment of histone deacetylases, transcriptional repression by nuclear receptors, modulation of estrogen receptor transcriptional activity via NCOA1, mitochondrial respiration activity, and aging (Delage-Mourroux *et al.*, 2000). Furthermore, both prohibitins have been shown to be activated by c-*myc* and to have important roles in the control of apoptosis (O'Connell *et al.*, 2003).

Another protein regulating cell proliferation which was upregulated in GST-P$^+$ foci and HCCs is SEPT9. Highly expressed in neuronal tissues and breast cancer and a member of the cytoskeleton-related septin family, SEPT9, has been shown to be involved in cytokinesis, cell survival, and to suppress apoptosis (Roeseler *et al.*, 2009). Its altered expression has been implicated in neoplasia (Ito *et al.*, 2005). SEPT9 accelerated growth kinetics, stimulated cell motility, promoted invasion in Matrigel Transwell assays, increased genomic instability with the development of aneuploidy, and stimulated morphologic changes. Furthermore, there is growing evidence for cross talk between septin filaments and actin cytoskeleton (F-actin) which is regulated by Rho family of GTPases (Ito *et al.*, 2005). Moreover, SEPT9 methylated DNA has become recently used as a biomarker for colorectal cancer (Grutzmann *et al.*, 2008).

Interestingly, overexpression of another neuronal tissue protein Neb1 was detected in GST-P$^+$ foci of rats in the PB promotion group. A mosaic staining pattern for Neb1 was also observed in rat HCCs. Similar to SEPT9, this protein phosphatase 1-alpha inhibitor has been shown to bind to actin filaments (F-actin), show cross-linking activity and be involved in neurite and synapse formation and function (Nakanishi *et al.*, 1997). Furthermore, coexpression of neurabin with Lfc (lymphoid blast crisis's first cousin), a Rho guanine nucleotide exchange factor has been demonstrated to result in their clustering together with F-actin, a process that depended on Rho activity (Ryan *et al.*, 2005). Thus, both SEPT9 and Neb1 are likely to be involved in Rho-dependent organization of F-actin which might be a link between the microtubule, intermediate filaments, and F-actin cytoskeletons. Their role in liver preneoplasia needs further investigation.

The results of this study confirmed our recent demonstration of elevation of CK8 and CK18 expression in rat liver preneoplastic lesions leading to intermediate filament reorganization involving histone H2aa3 in the GST-P$^+$ foci of rats treated with DEN and PB (Kakehashi *et al.*, 2009). Moreover, overexpression of histone H2be was detected which might also play role in intermediate filament reorganization. Recently, CK8 and CK18 were reported to bind to the cytoplasmic domain of tumor necrosis factor receptor 2 (TNFR2) and moderate tumor necrosis factor (TNF) related to JNK intracellular signaling and NF-κB activation. This influence on TNF, a cytokine produced by macrophages and T lymphocytes affecting cellular proliferation, survival, differentiation, and cell death, may be the fundamental function of CK8 and CK18 common to liver regeneration and the reason for the persistent expression of these CKs in many carcinomas (Caulin *et al.*, 2000).

In the present experiment, cellular transporters APOA1, APOE, and A2M, secreted proteins detected in blood serum, plasma, and urine, were overexpressed in both GST-P$^+$ foci and HCCs. APOE and APOA1 are the proteins mediating binding, internalization, and catabolism of lipoprotein particles. APOE participates in Akt phosphorylation and can serve as a ligand for the low density lipoprotein (apo-B/E) receptor and for the specific apo-E receptor of hepatic tissues being overexpressed in response to reactive oxygen species (Fazio *et al.*, 2000). A2M, a cytokine transporter secreted in plasma, is able to inhibit all four classes of proteinases by a unique "trapping" mechanism (Sukata *et al.*, 2004). It has been reported to promote hepatocarcinogenesis by perturbing transforming growth factor-α–induced apoptosis. Elevation of A2M mRNA was detected in rat liver amphophilic cell foci induced by DEN and the peroxisomal proliferators Wy-14,643 or clofibrate (Sukata *et al.*, 2004).

An involvement of reactive oxygen species in the genesis of human cancers has been proposed, and a remarkable decrease of CAT mRNA levels and activity after immortalization and malignant transformation of mouse liver cells has been previously reported in line with our results (Sun *et al.*, 1993). The downregulation of CAT gene expression could be explained by a remarkable difference in methylation status of the CAT gene. Furthermore, CAT-negative hepatocytes did not show evidence of apoptosis or necrotic cell death (Oikawa and Novikoff, 1995). Similar to CAT, inhibition of PON1 was detected in both GST-P$^+$ foci and HCCs. PON1 is an arylesterase that mainly hydrolyzes the organophosphorus anticholinesterase compound paroxon to produce *p*-nitrophenol (Furlong, 2007). PON1 is also known to regulate lipid metabolic processes and be involved in responses to external stimuli, positively regulating cholesterol efflux and catabolism of aromatic compounds.

Urea cycle metabolic enzymes expression was here found suppressed in the GST-P$^+$ foci of both initiation control and PB-administered animals. These included CPS1, OTC, and ASS1 which are involved in the urea cycle of ureotelic animals where they play important roles in removing excess ammonia from the cell. In line with our results, its downregulation was previously observed in human HCCs (Chaerkady *et al.*, 2008).

In conclusion, early coordinated elevation of mitochondrial prohibitins and SEPT9 associated with induction of Neb1,

APOE, APOA1, A2M, PGRMC1, H2aa3, and CK5, CK8, CK13, CK14, CK17, and CK18, induction of cell proliferation, and suppression of detoxification system and urea cycle enzymes in areas of GST-P$^+$ foci suggested their involvement in onset and promotion of rat hepatocarcinogenesis leading to the development of HCCs. Combination of laser microdissection, QSTAR Elite LC-MS/MS, and iTRAQ technology thus might become a powerful tool for protein spectrum analysis, facilitating the search for mechanisms of carcinogenesis and identifying potential biomarkers for liver preneoplasia for early diagnosis.

FUNDING

Ministry of Health, Labor and Welfare of Japan [Grant-in-Aid for Scientific Research 19710167].

ACKNOWLEDGMENTS

We thank Masayo Inoue, Kaori Touma, and Rie Onodera for their technical assistance and Yukiko Iura for her help during preparation of this article.

REFERENCES

Caulin, C., Ware, C. F., Magin, T. M., and Oshima, R. G. (2000). Keratin-dependent, epithelial resistance to tumor necrosis factor-induced apoptosis. *J. Cell Biol.* **149,** 17–22.

Carlson, D. B., and Perdew, G. H. (2002). A dynamic role for the Ah receptor in cell signaling? Insights from a diverse group of Ah receptor interacting proteins. *J. Biochem. Mol. Toxicol.* **16,** 317–325.

Chaerkady, R., Harsha, H. C., Nalli, A., Gucek, M., Vivekanandan, P., Akhtar, J., Cole, R. N., Simmers, J., Schulick, R. D., Singh, S., *et al.* (2008). A quantitative proteomic approach for identification of potential biomarkers in hepatocellular carcinoma. *J. Proteome Res.* **7,** 4289–4298.

Choi, D., Lee, S. J., Hong, S., Kim, I. H., and Kang, S. (2008). Prohibitin interacts with RNF2 and regulates E2F1 function via dual pathways. *Oncogene* **27,** 1716–1725.

Delage-Mourroux, R., Martini, P. G., Choi, I., Kraichely, D. M., Hoeksema, J., and Katzenellenbogen, B. S. (2000). Analysis of estrogen receptor interaction with a repressor of estrogen receptor activity (REA) and the regulation of estrogen receptor transcriptional activity by REA. *J. Biol. Chem.* **275,** 35848–35856.

Fazio, S., Linton, M. F., and Swift, L. L. (2000). The cell biology and physiologic relevance of ApoE recycling. *Trends Cardiovasc. Med.* **10,** 23–30.

Furlong, C. E. (2007). Genetic variability in the cytochrome P450-paraoxonase 1 (PON1) pathway for detoxication of organophosphorus compounds. *J. Biochem. Mol. Toxicol.* **21,** 197–205.

Fusaro, G., Wang, S., and Chellappan, S. (2002). Differential regulation of Rb family proteins and prohibitin during camptothecin-induced apoptosis. *Oncogene* **21,** 4539–4548.

Gluckmann, M., Fella, K., Waidelich, D., Merkel, D., Kruft, V., Kramer, P. J., Walter, Y., Hellmann, J., Karas, M., and Kroger, M. (2007). Prevalidation of potential protein biomarkers in toxicology using iTRAQ reagent technology. *Proteomics* **7,** 1564–1574.

Grutzmann, R., Molnar, B., Pilarsky, C., Habermann, J. K., Schlag, P. M., Saeger, H. D., Miehlke, S., Stolz, T., Model, F., Roblick, U. J., *et al.* (2008). Sensitive detection of colorectal cancer in peripheral blood by septin 9 DNA methylation assay. *PLoS One* **3,** e3759.

Ito, H., Iwamoto, I., Morishita, R., Nozawa, Y., Narumiya, S., Asano, T., and Nagata, K. (2005). Possible role of Rho/Rhotekin signaling in mammalian septin organization. *Oncogene* **24,** 7064–7072.

Ito, N., Hasegawa, R., Imaida, K., Masui, T., Takahashi, S., and Shirai, T. (1992). Pathological markers for non-genotoxic agent-associated carcinogenesis. *Toxicol. Lett.* 64–65, Spec No. 613–620.

Kakehashi, A., Inoue, M., Wei, M., Fukushima, S., and Wanibuchi, H. (2009). Cytokeratin 8/18 overexpression and complex formation as an indicator of GST-P positive foci transformation into hepatocellular carcinomas. *Toxicol. Appl. Pharmacol.* **238,** 71–79.

Kakehashi, A., Kato, A., Inoue, M., Ishii, N., Okazaki, E., Wei, M., Tachibana, T., and Wanibuchi, H. (2010). Cytokeratin 8/18 as a new marker of mouse liver preneoplastic lesions. *Toxicol. Appl. Pharmacol.* **242,** 47–55.

Kensler, T. W., and Wakabayashi, N. (2010). Nrf2: friend or foe for chemoprevention? *Carcinogenesis* **31,** 90–99.

Kinoshita, A., Wanibuchi, H., Imaoka, S., Ogawa, M., Masuda, C., Morimura, K., Funae, Y., and Fukushima, S. (2002). Formation of 8-hydroxydeoxyguanosine and cell-cycle arrest in the rat liver via generation of oxidative stress by phenobarbital: association with expression profiles of p21(WAF1/Cip1), cyclin D1 and Ogg1. *Carcinogenesis* **23,** 341–349.

Kitano, M., Ichihara, T., Matsuda, T., Wanibuchi, H., Tamano, S., Hagiwara, A., Imaoka, S., Funae, Y., Shirai, T., and Fukushima, S. (1998). Presence of a threshold for promoting effects of phenobarbital on diethylnitrosamine-induced hepatic foci in the rat. *Carcinogenesis* **19,** 1475–1480.

Malhotra, D., Portales-Casamar, E., Singh, A., Srivastava, S., Arenillas, D., Happel, C., Shyr, C., Wakabayashi, N., Kensler, T. W., Wasserman, W. W., *et al.* (2010). Global mapping of binding sites for Nrf2 identifies novel targets in cell survival response through ChIP-Seq profiling and network analysis. *Nucleic Acids Res* **9,** 5718–5734.

Melle, C., Kaufmann, R., Hommann, M., Bleul, A., Driesch, D., Ernst, G., and von Eggeling, F. (2004). Proteomic profiling in microdissected hepatocellular carcinoma tissue using ProteinChip technology. *Int. J. Oncol.* **24,** 885–891.

Merkwirth, C., Dargazanli, S., Tatsuta, T., Geimer, S., Lower, B., Wunderlich, F. T., von Kleist-Retzow, J. C., Waisman, A., Westermann, B., and Langer, T. (2008). Prohibitins control cell proliferation and apoptosis by regulating OPA1-dependent cristae morphogenesis in mitochondria. *Genes Dev.* **22,** 476–488.

Nakanishi, H., Obaishi, H., Satoh, A., Wada, M., Mandai, K., Satoh, K., Nishioka, H., Matsuura, Y., Mizoguchi, A., and Takai, Y. (1997). Neurabin: a novel neural tissue-specific actin filament-binding protein involved in neurite formation. *J. Cell Biol.* **139,** 951–961.

Nijtmans, L. G., Artal, S. M., Grivell, L. A., and Coates, P. J. (2002). The mitochondrial PHB complex: roles in mitochondrial respiratory complex assembly, ageing and degenerative disease. *Cell Mol. Life Sci.* **59,** 143–155.

O'Connell, B. C., Cheung, A. F., Simkevich, C. P., Tam, W., Ren, X., Mateyak, M. K., and Sedivy, J. M. (2003). A large scale genetic analysis of c-Myc-regulated gene expression patterns. *J. Biol. Chem.* **278,** 12563–12573.

Oikawa, I., and Novikoff, P. M. (1995). Catalase-negative peroxisomes: transient appearance in rat hepatocytes during liver regeneration after partial hepatectomy. *Am. J. Pathol.* **146,** 673–687.

Roeseler, S., Sandrock, K., Bartsch, I., and Zieger, B. (2009). Septins, a novel group of GTP-binding proteins: relevance in hemostasis, neuropathology and oncogenesis. *Klin. Padiatr.* **221,** 150–155.

Ryan, X. P., Alldritt, J., Svenningsson, P., Allen, P. B., Wu, G. Y., Naim, A. C., and Greengard, P. (2005). The Rho-specific GEF Lfc interacts with neurabin and spinophilin to regulate dendritic spine morphology. *Neuron* **47,** 85–100.

Seow, T. K., Ong, S. E., Liang, R. C., Ren, E. C., Chan, L., Ou, K., and Chung, M. C. (2000). Two-dimensional electrophoresis map of the human hepatocellular carcinoma cell line, HCC-M, and identification of the separated proteins by mass spectrometry. *Electrophoresis* **21,** 1787–1813.

Sukata, T., Uwagawa, S., Ozaki, K., Sumida, K., Kikuchi, K., Kushida, M., Saito, K., Morimura, K., Oeda, K., Okuno, Y., *et al.* (2004). Alpha(2)-macroglobulin: a novel cytochemical marker characterizing preneoplastic and neoplastic rat liver lesions negative for hitherto established cytochemical markers. *Am. J. Pathol.* **165,** 1479–1488.

Sun, Y., Colburn, N. H., and Oberley, L. W. (1993). Depression of catalase gene expression after immortalization and transformation of mouse liver cells. *Carcinogenesis* **14,** 1505–1510.

Tachibana, T., Okazaki, E., Yoshimi, T., Azuma, M., Kakehashi, A., and Wanibuchi, H. (2010). Rat monoclonal antibody specific for septin 9. *Hybridoma (Larchmt)* **29,** 169–171.

Tatsuta, T., Model, K., and Langer, T. (2005). Formation of membrane-bound ring complexes by prohibitins in mitochondria. *Mol. Biol. Cell* **16,** 248–259.

Theiss, A. L., Idell, R. D., Srinivasan, S., Klapproth, J. M., Jones, D. P., Merlin, D., and Sitaraman, S. V. (2007). Prohibitin protects against oxidative stress in intestinal epithelial cells. *FASEB J.* **21,** 197–206.

Wakabayashi, N., Slocum, S. L., Skoko, J. J., Shin, S., and Kensler, T. W. (2010). When NRF2 talks, who's listening? *Antioxid Redox Signal* **13,** 1649–1663.

TOXICOLOGICAL SCIENCES **125(2)**, 392–400 (2012)
doi:10.1093/toxsci/kfr314
Advance Access publication November 17, 2011

2-Amino-3-Methylimidazo[4,5-*f*]Quinoline (IQ) Promotes Mouse Hepatocarcinogenesis by Activating Transforming Growth Factor-β and Wnt/β-Catenin Signaling Pathways

Xiao-Li Xie, Min Wei, Anna Kakehashi, Shotaro Yamano, Masaki Tajiri, and Hideki Wanibuchi[1]

Department of Pathology, Graduate School of Medicine, Osaka City University, Osaka 545-8585, Japan

[1]To whom correspondence should be addressed at Department of Pathology, Graduate School of Medicine, Osaka City University, Asahi-machi 1-4-3, Abeno-ku, Osaka 545-8585, Japan. Fax: +816-6646-3093. E-mail: wani@med.osaka-cu.ac.jp.

Received September 14, 2011; accepted November 11, 2011

The purposes of the present study were to investigate the modifying effects of 2-amino-3-methylimidazo[4,5-*f*]quinoline (IQ), a genotoxic carcinogen produced during cooking of protein-rich foods, and elucidate underlying mechanisms in a two-stage hepatocarcinogenesis mice model. Six-week-old B6C3F1 mice were subjected to two-thirds partial hepatectomy at the beginning of the study, followed by an intraperitoneal injection of diethylnitrosamine on day 1. Starting 1 week later, they were fed diets containing IQ at doses of 30, 100, or 300 ppm for 39 weeks. A dose-dependent trend for increase in eosinophilic altered foci as well as eosinophilic hepatocellular adenomas was observed, along with significant elevation in the incidence of hepatocellular carcinomas in the 100- and 300-ppm IQ groups as compared with initiation control group. Furthermore, IQ elevated the protein expression levels of Wnt1, transforming growth factor-β (TGF-β), TGF-β receptors 1 and 2 (TβR1 and TβR2), and phosphorylated c-Jun (p-c-Jun), while suppressing those of E-cadherin and $p21^{WAF1/Cip1}$. Moreover, translocation of β-catenin to the nuclei as well as upregulated nuclear expression of c-Myc and cyclin D1, which are downstream targets of β-catenin and p-c-Jun, were detected at 100 and 300 ppm. These findings suggest that IQ exerts dose-dependent promoting effects on mice hepatocarcinogenesis by activating TGF-β and Wnt/β-catenin signaling pathways and inhibiting cell adhesion.

Key Words: **IQ; hepatocarcinogenesis; TGF-β pathway; Wnt/β-catenin pathway; E-cadherin.**

The incidence of hepatocellular carcinomas (HCCs) has significantly increased over the past decades, attribute to the increased prevalence of chronic liver hepatitis, especially chronic hepatitis B and C, whereas some other factors, such as dietary carcinogens, also contribute to the risk of certain types of cancer (Glade, 1999). Epidemiological studies have found a positive correlation between dietary intake of foodstuffs containing traces of heterocyclic amines and the likelihood of developing cancer (Layton *et al.*, 1995). In the human diet, consumption of 400 g of cooked lean meat could result in exposure to several micrograms of mutagenic heterocyclic amines (Lakshmi *et al.*, 2008). These amines can be detected in urine and their excretion as unchanged forms is increased by cytochrome P450 (P450) inhibition (Turesky *et al.*, 2002), indicating absorption from cooked foods and P450 metabolism. 2-Amino-3-methylimidazo[4,5-*f*]quinoline (IQ), one of the genotoxic and carcinogenic heterocyclic amines formed by high-temperature cooking of proteinaceous food, targets multiple organs in rodents. For example, long-term treatment (675 days) with 300 ppm IQ has been shown to induce tumors in the liver, lung, and forestomach of CDF1 mice (Ohgaki *et al.*, 1986).

The mutagenicity and carcinogenicity of IQ are considered initially to involve oxidation of the exocyclic amino group (G) to its corresponding N-hydroxyl-IQ by liver CYP1A1 and 1A2 (Hammons *et al.*, 1997). Subsequently, *O*-acetylation or sulfonation of the exocyclic group is believed to result in the formation of the ultimate genotoxic species, which are capable of binding to DNA, leading to formation of DNA adducts, and in turn mutations and neoplastic transformation (Lakshmi *et al.*, 2008; Turesky *et al.*, 2002). It has also been reported that IQ is associated with *p53* gene mutations in HCCs in the cynomolgus monkey. It was further suggested that these mutations might be induced by the formation of DNA adducts of IQ in the *p53* gene (Fujimoto *et al.*, 1994). Moreover, IQ may suppress the activity of protein kinase C and blockade activation of nuclear factor-kappaB and AP-1 with IL-2 gene expression in murine spleen cells (Lee *et al.*, 1998). However, despite the fact that daily exposure to IQ and other heterocyclic amines in food may present a potent carcinogenic risk to humans, the mechanisms underlying IQ carcinogenicity are still not fully understood.

In recent years, transforming growth factor-beta (TGF-β), E-cadherin adhesion complexes, and the Wnt/β-catenin pathways have become hot topics in HCCs studies (Marijon *et al.*, 2011; Matsuzaki *et al.*, 2007; Polakis, 2000; Sekimoto *et al.*, 2007; Wolfe *et al.*, 2011). TGF-β and its isoforms initiate a

signaling cascade, which is closely linked to liver fibrosis, cirrhosis, and subsequent progression to HCCs, thus playing a unique role in its molecular pathogenesis (Giannelli *et al.*, 2011). However, it is not clear whether there is any relationship between IQ and TGF-β or its isoforms during hepatocarcinogenesis.

β-Catenin is an E-cadherin-binding protein involved in cell-cell adhesion (Hirohashi, 1998), but it also functions as a transcriptional activator in the Wnt pathway when assembled in the nucleus with members of the T lymphocyte-specific transcription factor/lymphoid enhancer-binding factor family of binding proteins (Korinek *et al.*, 1998). It may also be a target of IQ, which can induce β-catenin mutations in rat colon tumors, which feature elevated expression of c-Myc and c-Jun proteins (Blum *et al.*, 2001). Whether IQ exerts effects on β-catenin and related factors in hepatocarcinogenesis remains to be clarified.

As the metabolism of IQ in the mouse is similar to human (Lakshmi *et al.*, 2008), in the present study, we chose a two-stage mouse model to investigate the effects of different doses of IQ on hepatocarcinogenesis, focusing on underlying mechanisms involving the above-mentioned pathways.

MATERIALS AND METHODS

Chemicals and diets. IQ was purchased from the Nard Institute (Osaka, Japan), with a purity of 99.9%, and diethylnitrosamine (DEN) from Tokyo Chemical Industry Company (Tokyo, Japan). Basal diet (powdered MF; Oriental Yeast Co., Tokyo, Japan) was prepared once a month by Oriental Yeast Co. The diets containing IQ were made once a month using a roller (Universal Ball Mill UB32; Yamato Scientific Co., Tokyo, Japan) and draft chamber (GHD-1500; Oriental Giken Inc., Tokyo, Japan) set in the animal center.

Animals and procedures. One hundred and forty-five 5-week-old male B6C3F1 mice (Charles River, Shizuoka, Japan) were housed in plastic cages (five animals per cage) in an animal facility maintained under standard conditions (room temperature, 23 ± 1°C; relative humidity, 44 ± 5%; and light/dark cycle, 12 h) and were given free access to powdered diet (Oriental MF; Oriental Yeast Co.) and tap water. The animals were acclimatized for 1 week prior to the beginning of the experiment, which was conducted after obtaining approval of the Animal Care and Use Committee of Osaka City University Medical School.

The experimental protocol is shown in Figure 1. To enhance hepatocellular proliferation, two-thirds partial hepatectomy (PH) was performed in 105 mice, under anesthesia as previously described (Nicou *et al.*, 2007). Briefly, after ventral laparotomy, the left lateral, left median, and right median lobes were ligated and excised. Twenty-four hours after the PH, 105 mice were randomly divided into six groups. Seventy-five mice in groups 1–4 (G1–G4) underwent a single intraperitoneal injection of DEN (30 mg/kg body weight) and 30 mice in groups 5–6 (G5 and G6) were given an equal volume of saline instead. The other 40 mice not subjected to PH were divided into two groups (G7 and G8) after ip injection of DEN. Starting 1 week after initiation, animals were administered 0, 30, 100, or 300 ppm IQ in the diet for 39 weeks.

Tumor harvest. At sacrifice, all hepatic lobes were cut into slices and fixed in 10% phosphate-buffered formalin for histopathological examination. Macroscopically evident nodules with a diameter larger than 3 mm were each cut in two halves, one fixed in 10% phosphate-buffered formalin for histopathological and immunohistochemical analyses and the other frozen in liquid nitrogen and stored at −80°C for molecular analyses.

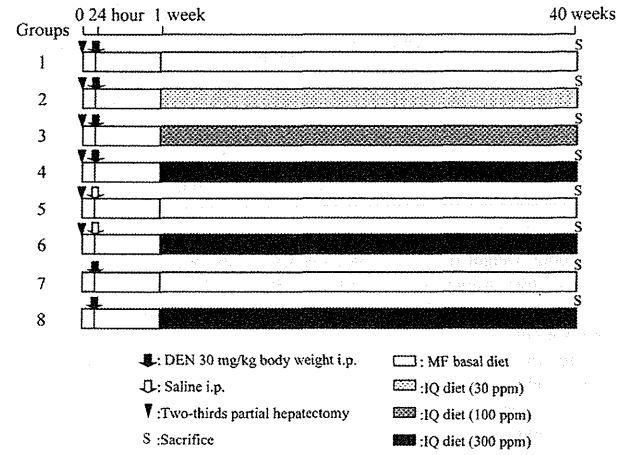

FIG. 1. Experimental design for the two-stage mouse hepatocarcinogenesis model. The numbers of mice from groups 1 to 8 were 20, 20, 20, 15, 10, 20, 20, and 20, respectively.

Histopathology. After formalin fixation, livers were embedded in paraffin, sectioned at 3-μm thickness, and stained with hematoxylin and eosin (H&E) for histopathological examination. Liver altered foci, hepatic adenomas, and HCCs were counted under the light microscope and categorized based on tumor size, thickness of hepatic plates, and presence of mitotic figures, according to the diagnostic criteria provided by Maronpot *et al.* (1999).

Immunohistochemistry. Immunohistochemical analyses were performed on liver tumors, hepatocellular adenomas (HCAs) and HCCs, of mice in PH→DEN groups as described previously (Kakehashi *et al.*, 2010). In this study, we employed primary antibodies against β-catenin (dilution 1:100, 6B3; Cell Signaling Technology, Beverly, New York), TGF-β (dilution 1:500, ab66043; Abcam Inc., Cambridge, MA), E-cadherin (dilution 1:500, ab53033; Abcam), Wnt1 (dilution 1:200, ab15251; Abcam), and c-Myc (dilution 1:100, ab39688; Abcam). After testing the different antigen-retrieval methods and negative controls, immunohistochemical procedures were optimized.

Extraction of nuclear proteins and whole cell proteins. Three tumors in each group of animals that underwent PH followed by DEN injection were used for protein expression analysis. Nuclear protein mixtures were prepared with a Nuclear Extraction Kit (Panomics, Santa Clara, CA) according to the manufacturer's instructions. Whole cell proteins of the tumors were also extracted as described previously (Kang *et al.*, 2008).

Western blotting analysis. Supernatants obtained from mice liver tumors (20 μg protein per sample) were separated by SDS-polyacrylamide gel electrophoresis (PAGE) and transferred to polyvinylidine difluoride membranes. After blocking for 1 h in 5% milk-Tris-buffered solution-Tween solution, membranes were incubated with primary antibodies at 4°C overnight, followed by the appropriate secondary antibody for 1 h at room temperature. Bands were visualized using the ECL PLUS system (Amersham, U.K.). Primary antibodies against β-catenin (dilution 1:2000, 6B3; Cell Signaling Technology), TGF-β (dilution 1:1000, ab66043; Abcam Inc.), E-cadherin (dilution 1:2000, ab53033; Abcam), TGF-β receptor 1 (TβR1, dilution 1:1000, ab31013; Abcam) and TGF-β receptor 2 (TβR2, dilution 1:1000, ab53168; Abcam), Wnt1 (dilution 1:500, ab15251; Abcam), c-Myc (dilution 1:1000, ab39688; Abcam), $p21^{WAF1/Cip1}$ (dilution 1:1000, ab7960; Abcam), cyclin D1 (dilution 1:1000, sc-8396; Santa Cruz Biotechnology, Inc., Santa Cruz, CA), p53 (dilution 1:2000, sc-6243; Santa Cruz), phosphorylated c-Jun (p-c-Jun, dilution 1:1000, sc-16312; Santa Cruz), β-actin (dilution 1:10000, ab49900; Abcam), and histone H2A (acidic patch, dilutin 1:2000, 07-146; Upstate Biotechnology, Billerica, MA) were applied.

TABLE 1
Final Body Weights, Liver Weights, Water Intake, Food Consumption and IQ Intake of Mice

Groups	PH → DEN →				PH →		DEN →	
	— (G1)	30 ppm IQ (G2)	100 ppm IQ (G3)	300 ppm IQ (G4)	Saline (G5)	300 ppm IQ (G6)	— (G7)	300 ppm IQ (G8)
Number of effective mice	15	16	19	13	9	19	19	20
Final body weight (g)	38.23 ± 3.88	36.73 ± 3.40	35.88 ± 3.19	31.85 ± 3.02*	38.26 ± 3.08	32.81 ± 2.81**	35.75 ± 3.75	30.77 ± 2.07*
Absolute liver weight (g)	1.98 ± 0.52	1.79 ± 0.38	2.01 ± 0.77	1.70 ± 0.43	1.74 ± 0.38	1.47 ± 0.15	1.89 ± 0.20	1.56 ± 0.13*
Relative liver weight (%g/g body weight)	5.20 ± 1.36	4.85 ± 0.80	5.52 ± 1.69	5.40 ± 1.61	4.58 ± 1.11	4.48 ± 0.29	5.34 ± 0.81	5.09 ± 0.57
Average food intake (g/g body weight/day)	0.12 ± 0.02	0.13 ± 0.03	0.13 ± 0.03	0.12 ± 0.02	0.11 ± 0.02	0.12 ± 0.02	0.13 ± 0.02	0.13 ± 0.02
Average IQ intake (μg/g body weight/day)	—	3.94 ± 0.84	12.92 ± 2.69	37.41 ± 5.61	—	35.81 ± 5.66	—	49.63 ± 7.04

Note. G, group.
*$p < 0.01$ versus DEN control group, respectively; **$p < 0.01$ versus saline control group.

Densitometric analysis was carried out using TINA software (Raytest, Straubenhardt, Germany) with β-actin used as a whole cell internal control and histone H2A as a nuclear internal control. Data of relative integrated density values of selected bands are shown as bar charts.

Statistical analysis. All mean values were expressed as means ± SDs. Statistical analyses were performed using the Statlight program (Yukms Co., Ltd, Tokyo, Japan). Incidences of liver lesions were compared using the Chi-squared test.

Homogeneity of variance was tested by the Bartlett test in PH→DEN groups. Differences in mean values between the control and IQ-treatment groups were evaluated by the two-tailed Dunnett's test when variance was homogeneous and the two-tailed Steel's test when variance was heterogeneous.

Homogeneity of variance was tested by the *F*-test in groups undergoing PH without DEN initiation and groups without PH. Differences in mean values between the control and IQ-treatment groups were evaluated by the two-tailed Student's *t*-test when variance was homogeneous and the two-tailed Aspin-Welch's *t*-test when variance was heterogeneous. *P* values less than 0.05 were considered significant.

RESULTS

Body and Liver Weights, Water Intake, Food Consumption, and IQ Intakes

The results for body and liver weights, water intake, food consumption, and IQ intakes of mice are presented in Table 1. Eighteen animals in the initiation control and IQ-treated groups died during the study. Three mice each in G1 and G2, one mouse in G3, and two mice in G4 died from the hepatectomy operation during the first week after the start of the experiment. The causes of death of the other seven mice found dead are unclear, one mouse in G5 at week 3, one mouse each at weeks 15 and 19 in G1, one mouse in G2 at week 24, one mouse in G7 at week 25, and one mouse each at weeks 33 and 37 in G6. One mouse each in G3 and G4 died from liver extensive hemorrhage induced by tumors at weeks 36 and 38, respectively. As the first tumor was observed at week 36, all mice surviving until this week were included in the final analysis. IQ did not affect average food consumption and water intake, but suppressed body weight gain, mostly in the group administered the dose of 300 ppm.

In the groups undergoing PH followed by DEN initiation, final body weights of 300-ppm IQ-treated animals were significantly decreased compared with the DEN control group. No significant changes in final body weights were observed in the 30- and 100-ppm IQ groups. Similarly, final body weights of mice subjected to PH without DEN initiation followed by IQ administration at a dose of 300 ppm were significantly lower than that in the vehicle control group. Moreover, in the groups without PH, significant decrease of final body weight was observed at 300 ppm.

No significant changes in absolute and relative liver weights were observed in mice receiving IQ after PH with DEN initiation compared with the DEN control group. Furthermore, no significant changes of liver weights were found in animals subjected to PH without DEN initiation followed by 300 ppm IQ. In groups without PH, significant decrease of absolute but not relative liver weight was noted in the 300-ppm IQ group compared with the DEN control group.

Histopathological Evaluation

The results of the histopathological analysis are shown in Table 2. In mice undergoing PH with DEN initiation, 100- and 300-ppm IQ treatments significantly increased the development of HCCs, whereas in animals subjected to PH without DEN injection, no significant promoting effect of IQ was found. Thus, in the PH→DEN groups, incidence and multiplicity of HCCs with 100-ppm (33%, 0.33 ± 0.49) and 300-ppm (50%, 0.83 ± 1.19) IQ groups were significantly elevated as compared with the DEN control group (0%, 0 ± 0). In mice receiving 300 ppm IQ, multiplicity of total tumors (3.50 ± 2.11) was also significantly elevated compared with the initiation control group (1.73 ± 2.15). Furthermore, in the PH→DEN groups,

TABLE 2
Pathological Changes in Mouse Livers

Groups (number of group and effective mice)	PH → DEN → — (G1, 15)	PH → DEN → 30 ppm IQ (G2, 16)	PH → DEN → 100 ppm IQ (G3, 19)	PH → DEN → 300 ppm IQ (G4, 13)	PH → Saline (G5, 9)	PH → 300 ppm IQ (G6, 19)	DEN → — (G7, 19)	DEN → 300 ppm IQ (G8, 20)
Incidence of lesions (%)								
HCAs	12 (80)	13 (81.3)	14 (73.7)	12 (92.3)	0 (0)	2 (10.5)	0 (0)	0 (0)
HCCs	0 (0)	4 (25)	6 (33.3)*	6 (50)**	0 (0)	0 (0)	0 (0)	0 (0)
Total tumors	12 (80)	13 (81.3)	14 (73.7)	13 (100)	0 (0)	2 (10.5)	0 (0)	0 (0)
Multiplicity of lesions								
HCAs	1.73 ± 2.15	2.38 ± 2.59	2.47 ± 2.63	2.61 ± 1.33	0 ± 0	0.21 ± 0.63	0 ± 0	0 ± 0
HCCs	0 ± 0	0.31 ± 0.6	0.33 ± 0.49*	0.83 ± 1.19**	0 ± 0	0 ± 0	0 ± 0	0 ± 0
Total tumors	1.73 ± 2.15	2.69 ± 2.67	2.80 ± 2.93	3.45 ± 1.97*	0 ± 0	0.21 ± 0.63	0 ± 0	0 ± 0

Note. G, group.
*$p < 0.05$; **$p < 0.01$ versus DEN control group.

the rates for eosinophilic altered foci (control: 11.1%, 30 ppm IQ: 28.2%, 100 ppm IQ: 30.6%, 300 ppm IQ: 47.6%) and eosinophilic HCAs (control: 7.7%, 30 ppm IQ: 37.5%, 100 ppm IQ: 40.4%, 300 ppm IQ: 44.1%) showed a trend for dose-dependent increase, whereas the rates for basophilic altered foci and HCAs showed a decreasing trend (data not shown). Mixed type altered foci were not influenced by IQ application. No tumors were observed in animals not subjected to PH.

Effects of IQ on Protein Expression of E-Cadherin as Well as Components of TGF-β and Wnt/β-Catenin Signaling Pathways Found by Immunohistochemistry

In the liver tumors of all IQ-administered mice in PH→DEN groups, E-cadherin expression, a cell surface transmembrane glycoprotein with a key role not only in intracellular adhesion but also in cell differentiation, was significantly suppressed. Furthermore, in IQ-administered groups, E-cadherin was localized in the cytoplasm, whereas in the DEN initiation group, it was generally detected on the cell surfaces (Fig. 2a–d).

Protein expression of TGF-β, a known key regulator in HCCs development, was found to be elevated as compared with DEN control group tumors in all IQ-treatment groups (Fig. 2e–h).

In line with the findings for TGF-β, rise in protein expression of Wnt1, particularly in 300-ppm IQ-treated mice, but also present in 30- and 100-ppm IQ groups, was found as compared with the initiation control group (Fig. 2i–l).

β-Catenin membranous localization was observed in the liver tumors of DEN initiation control animals, whereas in IQ-treated mice, a shift to cytoplasmic and/or nuclear expression was found, most evident in the 100- and 300-ppm IQ-treatment groups (Fig. 2m–p). In parallel, c-Myc overexpression in the nuclei of tumor cells was also detected in mice administered IQ at 100 or 300 ppm (Fig. 2q–t).

Alteration in Protein Expression in Liver Tumors of Mice Detected by Western Blotting

Pronounced upregulation of TGF-β protein expression was found in the liver tumors of mice treated with IQ at doses of 100 ppm (1.45-fold) or 300 ppm (1.75-fold, Figure 3A). Furthermore, compared with the initiation control group, expressions of TβR1 and TβR2 were also enhanced by IQ, particularly at 300 ppm (2.01- and 2.10-fold, respectively). Expression of p-c-Jun, which can be stimulated by TGF-β, was also significantly increased in animals treated with 300 ppm IQ (1.57-fold, Fig. 3A). As with TGF-β and its receptors, expression of Wnt1 was also significantly elevated in 100- (1.95-fold) and 300-ppm (2.56-fold) IQ groups (Fig. 3A).

Similar to the results of immunohistochemical examination, expression of E-cadherin was significantly decreased in all IQ-treated animals, with the fold of 0.33, 0.22, and 0.24 from 30 to 300 ppm group, respectively, compared with the initiation control group (Fig. 3A).

Intriguingly, in the tumors of mice treated with 30–300 ppm IQ, a parabola-shaped change in protein expression levels of $p21^{WAF1/Cip1}$ was found. That is, compared with DEN control group, no change of $p21^{WAF1/Cip1}$ expression was observed in both high-dose IQ groups, whereas in the 30-ppm group, overexpression (1.37-fold) was clear (Fig. 3A).

Expression of p53 in the 300-ppm IQ-treatment group (2.56-fold) was significantly higher than in of initiation control group (Fig. 3A).

In the nuclei of liver tumor cells in mice administered 100 and 300 ppm IQ, overexpression of β-catenin (1.42- and 1.44-fold, respectively) was obvious compared with animals administered DEN alone (Fig. 3B), apparently coordinated with elevation of Wnt1 and suppression of E-cadherin. Expression of c-Myc (1.36- and 1.37-fold, respectively) and cyclin D1 (1.77- and 1.79-fold, respectively), the downstream of p-c-Jun and β-catenin, were also markedly increased by

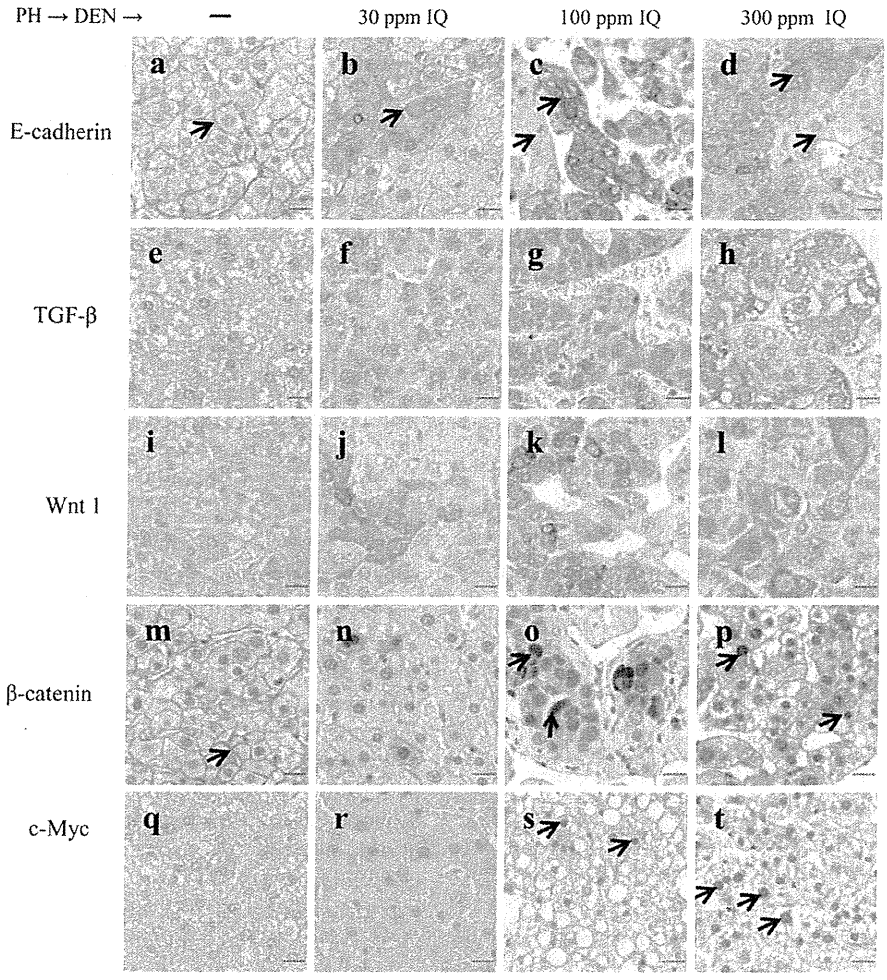

FIG. 2. Immunohistochemistry for E-cadherin (a–d), TGF-β (e–h), Wnt1 (i–l), β-catenin (m–p), and c-Myc (q–t) in the livers of mice. In the DEN control group (a), E-cadherin was located on the surfaces of tumor cells generally (arrow), whereas in IQ-treatment groups (b–d), it was decreased (arrow) and the localization was mostly cytoplasmic (arrow). Overexpression of TGF-β was detected in tumors of mice treated with IQ (f–h) compared with DEN alone (e). Wnt1 positivity in mouse liver tumors was also increased by IQ treatment (j–l), most prominently at 300 ppm (l) compared with the initiation control (i). β-Catenin showed membranous distribution in liver tumors of DEN control animals (m, arrow), but a shift to cytoplasmic/nucleus expression was observed in tumors of IQ-treatment groups, particularly in the 100- and 300-ppm IQ groups (o and p, arrow). Compared with the DEN control case (q), the numbers of c-Myc-positive nuclei were increased by IQ in the 100- and 300-ppm IQ groups (s and t, arrow). Bars represent 20 μm.

treatment with IQ at doses of 100 and 300 ppm when compared with the initiation control group (Fig. 3B).

DISCUSSION

This study provided the first evidence of promoting effects of 100 and 300 ppm IQ on liver carcinogenesis in male B6C3F1 mice. No significant influence of IQ compared with the PH alone control group was detected when mice were not initiated with DEN. In groups without PH, regardless of DEN injection and IQ treatment, no tumors were observed. However, in mice undergoing PH followed by DEN initiation, dose-dependent promotion effects of IQ on development of HCCs were clearly demonstrated. In this two-stage mouse model, not only DEN injection but also PH was necessary to detect the modifying effects of IQ on mice hepatocarcinogenesis. The progression step of hepatocarcinogenesis is irreversible and can be enhanced by administration of a "progressor," namely, a genotoxic compound (Dragan *et al.*, 1994). In rat liver carcinogenesis, most foci of altered hepatocytes, which finally progress to HCCs, are eosinophilic/clear cell foci (di Francesco *et al.*, 2007). In line with these data, administration of IQ, a genotoxic compound, dose-dependently increased eosinophilic altered foci and HCAs in the PH → DEN groups in this study. The augmentation of such lesions could clearly contribute to progression to HCCs.

Previous study demonstrated that administration of IQ alone, for almost 2 years, could straightforwardly increase liver tumor

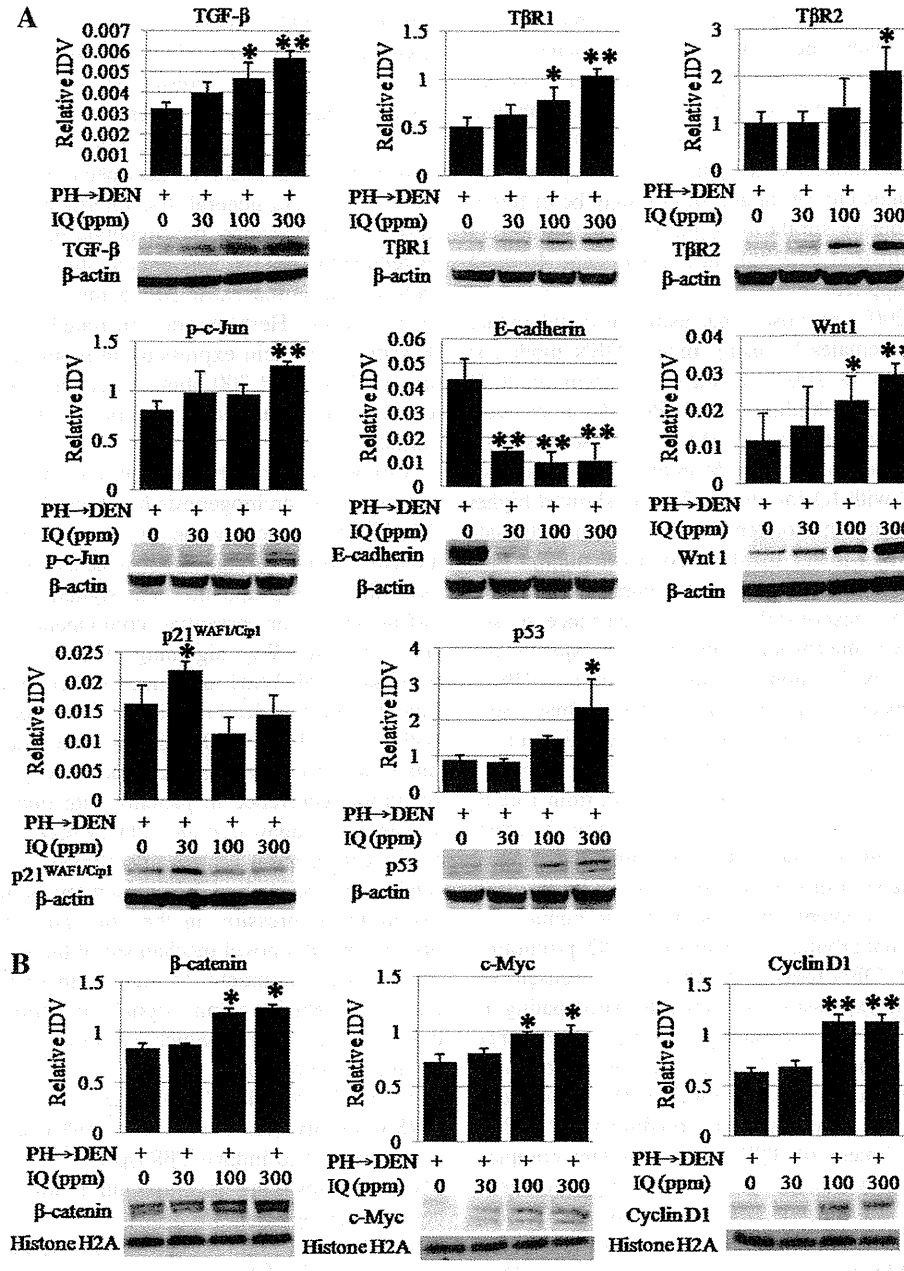

FIG. 3. Western blotting analysis of TGF-β, TβR1, TβR2, p-c-Jun, E-cadherin, Wnt1, $p21^{WAF1/Cip1}$, p53, β-catenin, c-Myc, and cyclin D1 protein expression in liver tumors of mice. (A) Compared with DEN initiation control group, significant overexpression of TGF-β (1.45- and 1.75-fold, respectively) and TβR1 (1.53- and 2.01-fold, respectively) was detected in the 100- and 300-ppm IQ groups. Protein expression of TβR2 (2.10-fold) and p-c-Jun (1.57-fold) was significantly increased only at 300 ppm. Significantly decreased expression levels of E-cadherin were observed in all IQ-treated animals, with the fold of 0.33, 0.22, and 0.24 from the 30-, 100-, and 300-ppm group, respectively, compared with the initiation control group. Expression levels of Wnt1 were significantly higher in IQ-administered groups, especially in the high-dose groups (2.56-fold). Significant overexpression of $p21^{WAF1/Cip1}$ was detected in the 30-ppm IQ group (1.37-fold), whereas no changes were found at the 100- and 300-ppm IQ doses. Increased expression of p53 was detected in mice treated with IQ at a dose of 300 ppm (2.56-fold). β-Actin was used as an internal control. (B) Compared with DEN initiation control group, overexpression of nuclear β-catenin (1.42- and 1.44-fold, respectively), c-Myc (1.36- and 1.37-fold, respectively), and cyclin D1 (1.77- and 1.79-fold, respectively) was detected in mice-administered IQ at doses of 100 and 300 ppm. Histone H2A was used as a nucleus internal control. Significant compared with the DEN alone group ($*p < 0.05$, $**p < 0.01$). IDV, integrated density value.

incidence in CDF1 mice and Fisher 344 (F344) rats (Ohgaki *et al.*, 1986). However, the underlying mechanisms of IQ effects have not been fully understood. Furthermore, because Lakshmi *et al.* (2008) pointed out that mouse IQ metabolism was similar to that for human but different from that for rat and the metabolism could influence tumorigenicity, the parameters affecting IQ tumorigenicity in rat and mouse may be different. In our study, considering similarity in the metabolism and the cost-effectiveness, instead of F344 rats, a two-stage 40-week mouse model was applied.

Naugler *et al.* (2007) proposed that estrogen could reduce liver cancer risk in females by using mouse DEN model, in which tumor appears in 100% of males but only in 13% females. In view of their findings, male B6C3F1 mice were chosen in our experiment because DEN was used as liver tumor initiation carcinogen after PH. Moreover, F344 male rats (68%) administered with IQ for almost 2 years showed higher incidence of HCCs than that of female (45%), although male CDF1 mice (41%) had lower incidence of liver tumors than that of female (75%, Ohgaki *et al.*, 1986). Furthermore, P450 enzymes, which were responsible for the occurrence of sex differences in rat liver microsomes, appear rather specifically depending on the sex hormones (Kamataki *et al.*, 1983). Considering the species variation and gender bias, sex-dependent effects induced by IQ need further investigation.

In the report by the World Health Organization of International Agency for Research on Cancer (1993), from 1 kg of cooked meats and fish, 0.02–158 μg of IQ was detected. Although the dosages used in the present experiment are several orders of magnitude apart from human consumption levels, daily exposure may present a potent carcinogenic risk to humans.

To elucidate the underlying mechanisms of IQ promoting effects in PH and DEN-treated animals, we focused on alterations in protein expression of elements participating in TGF-β and Wnt/β-catenin signaling. Emerging evidence indicates that TGF-β participates in oncogenic processes, such as growth stimulation and increased motility (Wakefield and Roberts, 2002). On the molecular level, binding of TGF-β to TβR2 leads to recruitment of TβR1. The resultant complex then triggers the downstream cascade to regulate gene transcription (Moustakas and Heldin, 2002). In the present study, dose-dependent increases of protein expression levels of TGF-β, TβR1, and TβR2 were observed in liver tumors of IQ-administered animals, thus indicating that IQ at high doses of 100 and 300 ppm activated the TGF-β signaling pathway. Moreover, eosinophilia may be caused by proliferation of mitochondria in rat hepatocytes (Reznik-Schuller and Gregg, 1983). Interestingly, protein TGF-β localizes in mitochondria (Heine *et al.*, 1991). Therefore, it is reasonable to speculate that enhanced expression of TGF-β might be related to the eosinophilic changes in IQ-treated groups in this study.

It has been previously reported that expression of E-cadherin, a cell surface transmembrane glycoprotein with a key role not only in intracellular adhesion but also in cell polarity, growth, and differentiation, is negatively regulated by TGF-β (Cano *et al.*, 2000). Dissociation of the E-cadherin adhesion complex is considered a prerequisite for tumor cell invasion and metastasis formation (Hirohashi, 1998; Wolfe *et al.*, 2011). Furthermore, loss of or reduced membrane positivity of E-cadherin has been described in HCCs (Wu *et al.*, 2011). In general, E-cadherin staining is strong in well-differentiated cancers that maintain their cell adhesiveness but is reduced in poorly differentiated tumors, which have lost cell-cell adhesion and show strong invasive behavior (Wijnhoven *et al.*, 2000). Here, we demonstrated significant inhibition of E-cadherin protein expression in mouse liver tumors by IQ at doses of 100 and 300 ppm, indicating that IQ treatment might enhance the malignant potential of tumor cells after DEN initiation.

Cooperation of the TGF-β and Wnt/β-catenin signaling pathways in carcinogenesis has been described (Takaku *et al.*, 1998). Thus, progression of benign adenomatous polyps to invasive forms of carcinoma is accelerated when members of both the TGF-β and the Wnt signaling cascades are altered. β-Catenin is an essential component of both intercellular junctions and Wnt signaling (Polakis, 2000). An increased expression of Wnt1 and nuclear accumulation of β-catenin have been recognized as features of an activated Wnt signaling pathway (Willert and Jones, 2006). In addition, a multivariate analysis earlier demonstrated poorer prognosis and higher rate of tumor recurrence in patients with nuclear accumulation of β-catenin (Inagawa *et al.*, 2002). Our finding of β-catenin translocation from plasma membranes to the cytoplasm and nucleus, associated with increased levels of Wnt1, c-Myc, and cyclin D1 expression in the 100- and 300-ppm IQ groups, points toward a novel mechanism of the promotion effect of IQ on HCCs development. In view of these results, we speculate that with Wnt/b-catenin signal activation, β-catenin targets c-Myc and cyclin D1, which leads to their upregulation, due to the influence of IQ.

TGF-β is capable of stimulating c-Jun NH_2-terminal kinase (JNK) activity (Hocevar *et al.*, 1999) and its activation has been reported to induce TβR1/$p21^{WAF1/Cip1}$ as well as JNK/c-Myc, thus resulting in either inhibition or promotion of rat hepatocarcinogenesis (Matsuzaki *et al.*, 2007; Sekimoto *et al.*, 2007). Here, we could demonstrate increased protein expression of $p21^{WAF1/Cip1}$ in the liver tumors of mice by 30 ppm IQ but no change with either the 100-ppm or the 300-ppm dosage. Furthermore, $p21^{WAF1/Cip1}$ suppression coordinated with overexpression of p-c-Jun was observed in tumors of the 100- and 300-ppm IQ-treatment groups. In line with our previous results, significant elevation of $p21^{WAF1/Cip1}$ was demonstrated with a low dose of IQ (10 ppm), even below that required for IQ-mediated carcinogenic effects in the liver of rats (Wei *et al.*, 2011). Moreover, suppression of $p21^{WAF1/Cip1}$ expression by 100- and 300-ppm doses of IQ might be suggested to be a result of an inhibitory effect on significantly upregulated c-Myc at these doses.

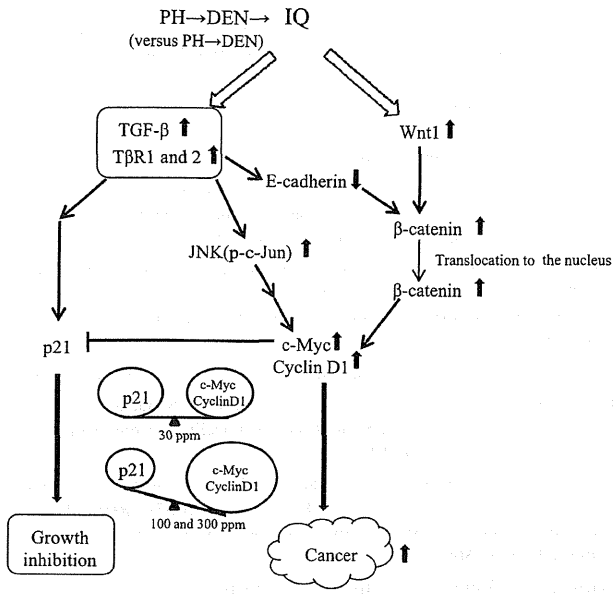

FIG. 4. Proposed model for IQ promotion mechanisms with regard to mouse hepatocarcinogenesis. IQ simultaneously stimulates TGF-β and Wnt signaling pathways in the two-stage mouse model. Increase in TGF-β complexes preponderantly stimulates JNK (p-c-Jun) and synchronously suppresses expression of E-cadherin. Subsequently, loss of E-cadherin expression results in translocation of β-catenin from cell surface to the cytoplasm and/or nucleus. At the same time, Wnt1 activates β-catenin and promotes its translocation. Thereafter, activation of downstream targets of β-catenin and TGF-β/JNK/c-Myc cascade, c-Myc and cyclin D1, results in promotion of HCCs development. Increased c-Myc may repress $p21^{WAF1/Cip1}$ expression, which indirectly suppresses cancer inhibition.

Expression of $p21^{WAF1/Cip1}$ can also be controlled by p53 (Wu *et al.*, 2003), for which overexpression has been found in many types of human malignancies. There is evidence supporting high levels of p53 alteration in HCCs (Guzman *et al.*, 2005) and significantly elevated expression was detected in the 300-ppm IQ group in the present study. The findings indicate that IQ affects the malignant progression of liver tumors with high levels of p53.

Because increased TGF-β and Wnt/β-catenin signaling have previously been associated with liver carcinogenesis (Polakis, 2000; Sekimoto *et al.*, 2007), the possibilities cannot be ruled out that latency-to-tumor is reduced after exposure to IQ and that tumors would have arisen anyway in the DEN initiation control group after 2 years and that these tumors would have the increased TGF-β and Wnt/β-catenin signaling. Nevertheless, in the present study, increased expressions of proteins TGF-β, TβR1, TβR2, Wnt1, p-c-Jun, p53 as well as nuclear proteins β-catenin, c-Myc, and cyclin D1 are at least partly responsible for dose-dependent promotion effects of IQ on mouse hepatocarcinogenesis when compared with these proteins expression profiles in the DEN initiation control group.

In conclusion, in the present study, IQ dose-dependently exerted promotion effects on mouse hepatocarcinogenesis. In this two-stage mouse model, the mechanism of IQ promotion effects on formation of HCCs appears likely to be related to the simultaneous stimulation of TGF-β and Wnt/β-catenin signaling pathways in hepatic tumors (Fig. 4). Increase of expression levels of TGF-β complex preponderantly stimulated JNK (p-c-Jun) and simultaneously suppressed expression of E-cadherin. The latter could have contributed to translocation of β-catenin from cell membranes to the cytoplasm and/or nucleus. Furthermore, increased expression of Wnt1 also might activate β-catenin and promote its translocation. Finally, induction of the downstream targets c-Myc and cyclin D1 occurred, resulting in the promotion of mouse hepatocarcinogenesis. Increased c-Myc may repress $p21^{WAF1/Cip1}$ expression, which indirectly suppresses cancer inhibition.

FUNDING

This work was supported by a grant-in-aid for scientific research from the Ministry of Health, Labor and Welfare of Japan.

ACKNOWLEDGMENTS

We thank Kaori Touma and Rie Onodera for their technical assistance and Yukiko Iura for her help during preparation of this manuscript.

REFERENCES

Blum, C. A., Xu, M., Orner, G. A., Fong, A. T., Bailey, G. S., Stoner, G. D., Horio, D. T., and Dashwood, R. H. (2001). beta-Catenin mutation in rat colon tumors initiated by 1,2-dimethylhydrazine and 2-amino-3-methylimidazo[4,5-f]quinoline, and the effect of post-initiation treatment with chlorophyllin and indole-3-carbinol. *Carcinogenesis* **22,** 315–320.

Cano, A., Perez-Moreno, M. A., Rodrigo, I., Locascio, A., Blanco, M. J., del Barrio, M. G., Portillo, F., and Nieto, M. A. (2000). The transcription factor snail controls epithelial-mesenchymal transitions by repressing E-cadherin expression. *Nat. Cell Biol.* **2,** 76–83.

di Francesco, F., Cautero, N., De Luca, S., Vecchi, A., Garelli, P., Doria, C., Marino, I. R., and Risaliti, A. (2007). Reconstruction of the suprahepatic cuff injured during multiorgan procurement using the infrahepatic vena cava of the liver allograft. *Liver Transpl.* **13,** 1468–1469.

Dragan, Y. P., Campbell, H. A., Baker, K., Vaughan, J., Mass, M., and Pitot, H. C. (1994). Focal and non-focal hepatic expression of placental glutathione S-transferase in carcinogen-treated rats. *Carcinogenesis* **15,** 2587–2591.

Fujimoto, Y., Hampton, L. L., Snyderwine, E. G., Nagao, M., Sugimura, T., Adamson, R. H., and Thorgeirsson, S. S. (1994). p53 gene mutation in hepatocellular carcinoma induced by 2-amino-3-methylimidazo[4,5-f]quinoline in nonhuman primates. *Jpn. J. Cancer Res.* **85,** 506–509.

Giannelli, G., Mazzocca, A., Fransvea, E., Lahn, M., and Antonaci, S. (2011). Inhibiting TGF-β signaling in hepatocellular carcinoma. *Biochim. Biophys. Acta* **1815,** 214–223.

Glade, M. J. (1999). Food, nutrition, and the prevention of cancer: A global perspective. American Institute for Cancer Research/World Cancer Research Fund, American Institute for Cancer Research, 1997. *Nutrition* **15,** 523–526.

Guzman, G., Alagiozian-Angelova, V., Layden-Almer, J. E., Layden, T. J., Testa, G., Benedetti, E., Kajdacsy-Balla, A., and Cotler, S. J. (2005). p53, Ki-67, and serum alpha feto-protein as predictors of hepatocellular carcinoma recurrence in liver transplant patients. *Mod. Pathol.* **18,** 1498–1503.

Hammons, G. J., Milton, D., Stepps, K., Guengerich, F. P., Tukey, R. H., and Kadlubar, F. F. (1997). Metabolism of carcinogenic heterocyclic and aromatic amines by recombinant human cytochrome P450 enzymes. *Carcinogenesis* **18,** 851–854.

Heine, U. I., Burmester, J. K., Flanders, K. C., Danielpour, D., Munoz, E. F., Roberts, A. B., and Sporn, M. B. (1991). Localization of transforming growth factor-beta 1 in mitochondria of murine heart and liver. *Cell Regul.* **2,** 467–477.

Hirohashi, S. (1998). Inactivation of the E-cadherin-mediated cell adhesion system in human cancers. *Am. J. Pathol.* **153,** 333–339.

Hocevar, B. A., Brown, T. L., and Howe, P. H. (1999). TGF-beta induces fibronectin synthesis through a c-Jun N-terminal kinase-dependent, Smad4-independent pathway. *EMBO J.* **18,** 1345–1356.

Inagawa, S., Itabashi, M., Adachi, S., Kawamoto, T., Hori, M., Shimazaki, J., Yoshimi, F., and Fukao, K. (2002). Expression and prognostic roles of beta-catenin in hepatocellular carcinoma: Correlation with tumor progression and postoperative survival. *Clin. Cancer Res.* **8,** 450–456.

Kakehashi, A., Kato, A., Inoue, M., Ishii, N., Okazaki, E., Wei, M., Tachibana, T., and Wanibuchi, H. (2010). Cytokeratin 8/18 as a new marker of mouse liver preneoplastic lesions. *Toxicol. Appl. Pharmacol.* **242,** 47–55.

Kamataki, T., Maeda, K., Yamazoe, Y., Nagai, T., and Kato, R. (1983). Sex difference of cytochrome P-450 in the rat: Purification, characterization, and quantitation of constitutive forms of cytochrome P-450 from liver microsomes of male and female rats. *Arch. Biochem. Biophys.* **225,** 758–770.

Kang, J. S., Wanibuchi, H., Morimura, K., Wongpoomchai, R., Chusiri, Y., Gonzalez, F. J., and Fukushima, S. (2008). Role of CYP2E1 in thioacetamide-induced mouse hepatotoxicity. *Toxicol. Appl. Pharmacol.* **228,** 295–300.

Korinek, V., Barker, N., Willert, K., Molenaar, M., Roose, J., Wagenaar, G., Markman, M., Lamers, W., Destree, O., and Clevers, H. (1998). Two members of the Tcf family implicated in Wnt/beta-catenin signaling during embryogenesis in the mouse. *Mol. Cell Biol.* **18,** 1248–1256.

Lakshmi, V. M., Hsu, F. F., and Zenser, T. V. (2008). N-Demethylation is a major route of 2-amino-3-methylimidazo[4,5-f]quinoline metabolism in mouse. *Drug Metab. Dispos.* **36,** 1143–1152.

Layton, D. W., Bogen, K. T., Knize, M. G., Hatch, F. T., Johnson, V. M., and Felton, J. S. (1995). Cancer risk of heterocyclic amines in cooked foods: An analysis and implications for research. *Carcinogenesis* **16,** 39–52.

Lee, Y. W., Han, S. H., Suh, J. H., Jeon, Y. J., and Yang, K. H. (1998). Down-regulation of protein kinase C: A potential mechanism for 2-amino-3-methylimidazo[4,5-f]quinoline-mediated immunosuppression. *Toxicol. Lett.* **102–103,** 79–83.

Marijon, H., Dokmak, S., Paradis, V., Zappa, M., Bieche, I., Bouattour, M., Raymond, E., and Faivre, S. (2011). Epithelial-to-mesenchymal transition and acquired resistance to sunitinib in a patient with hepatocellular carcinoma. *J. Hepatol.* **54,** 1073–1078.

Maronpot, R. R., Boorman, G. A., and Gaul, B. W. (1999). *Pathology of the Mouse.* Cache River Press, Vienna, IL.

Matsuzaki, K., Murata, M., Yoshida, K., Sekimoto, G., Uemura, Y., Sakaida, N., Kaibori, M., Kamiyama, Y., Nishizawa, M., Fujisawa, J., *et al.* (2007). Chronic inflammation associated with hepatitis C virus infection perturbs hepatic transforming growth factor beta signaling, promoting cirrhosis and hepatocellular carcinoma. *Hepatology* **46,** 48–57.

Moustakas, A., and Heldin, C. H. (2002). From mono- to oligo-Smads: The heart of the matter in TGF-beta signal transduction. *Genes Dev.* **16,** 1867–1871.

Naugler, W. E., Sakurai, T., Kim, S., Maeda, S., Kim, K., Elsharkawy, A. M., and Karin, M. (2007). Gender disparity in liver cancer due to sex differences in MyD88-dependent IL-6 production. *Science* **317,** 121–124.

Nicou, A., Serriere, V., Hilly, M., Prigent, S., Combettes, L., Guillon, G., and Tordjmann, T. (2007). Remodelling of calcium signalling during liver regeneration in the rat. *J. Hepatol.* **46,** 247–256.

Ohgaki, H., Hasegawa, H., Kato, T., Suenaga, M., Ubukata, M., Sato, S., Takayama, S., and Sugimura, T. (1986). Carcinogenicity in mice and rats of heterocyclic amines in cooked foods. *Environ. Health Perspect.* **67,** 129–134.

Polakis, P. (2000). Wnt signaling and cancer. *Genes Dev.* **14,** 1837–1851.

Reznik-Schuller, H. M., and Gregg, M. (1983). Sequential morphologic changes during methapyrilene-induced hepatocellular carcinogenesis in rats. *J. Natl. Cancer Inst.* **71,** 1021–1031.

Sekimoto, G., Matsuzaki, K., Yoshida, K., Mori, S., Murata, M., Seki, T., Matsui, H., Fujisawa, J., and Okazaki, K. (2007). Reversible Smad-dependent signaling between tumor suppression and oncogenesis. *Cancer Res.* **67,** 5090–5096.

Takaku, K., Oshima, M., Miyoshi, H., Matsui, M., Seldin, M. F., and Taketo, M. M. (1998). Intestinal tumorigenesis in compound mutant mice of both Dpc4 (Smad4) and Apc genes. *Cell* **92,** 645–656.

Turesky, R. J., Guengerich, F. P., Guillouzo, A., and Langouet, S. (2002). Metabolism of heterocyclic aromatic amines by human hepatocytes and cytochrome P4501A2. *Mutat. Res.* **506–507,** 187–195.

Wakefield, L. M., and Roberts, A. B. (2002). TGF-beta signaling: Positive and negative effects on tumorigenesis. *Curr. Opin. Genet. Dev.* **12,** 22–29.

Wei, M., Wanibuchi, H., Nakae, D., Tsuda, H., Takahashi, S., Hirose, M., Totsuka, Y., Tatematsu, M., and Fukushima, S. (2011). Low-dose carcinogenicity of 2-amino-3-methylimidazo[4,5-f]quinoline in rats: Evidence for the existence of no-effect levels and a mechanism involving $p21^{Cip\,/\,WAF1}$. *Cancer Sci.* **102,** 88–94.

Wijnhoven, B. P., Dinjens, W. N., and Pignatelli, M. (2000). E-cadherin-catenin cell-cell adhesion complex and human cancer. *Br. J. Surg.* **87,** 992–1005.

Willert, K., and Jones, K. A. (2006). Wnt signaling: Is the party in the nucleus? *Genes Dev.* **20,** 1394–1404.

Wolfe, A., Thomas, A., Edwards, G., Jaseja, R., Guo, G. L., and Apte, U. (2011). Increased activation of the Wnt/beta-catenin pathway in spontaneous hepatocellular carcinoma observed in farnesoid X receptor knockout mice. *J. Pharmacol. Exp. Ther.* **338,** 12–21.

World Health Organization of International Agency for Research on Cancer. (1993). *IQ (2-AMINO-3-METHYLIMIDAZO[4,5-f]QUINOLINE). IARC Monographs on the Evaluation of Carcinogenic Risks to Humans: Some Naturally Occurring Substances: Food Items and Constituents, Heterocyclic Aromatic Amines and Mycotoxins,* Vol. 56, pp. 165–195. IARC, Lyon, France.

Wu, J., Ru, N. Y., Zhang, Y., Li, Y., Wei, D., Ren, Z., Huang, X. F., Chen, Z. N., and Bian, H. (2011). HAb18G/CD147 promotes epithelial-mesenchymal transition through TGF-beta signaling and is transcriptionally regulated by Slug. *Oncogene* **30,** 4410–4427.

Wu, S., Cetinkaya, C., Munoz-Alonso, M. J., von der Lehr, N., Bahram, F., Beuger, V., Eilers, M., Leon, J., and Larsson, L. G. (2003). Myc represses differentiation-induced $p21^{CIP1}$ expression via Miz-1-dependent interaction with the p21 core promoter. *Oncogene* **22,** 351–360.

DDX39 acts as a suppressor of invasion for bladder cancer

Minoru Kato,[1,2] Min Wei,[1] Shotaro Yamano,[1] Anna Kakehashi,[1] Satoshi Tamada,[2] Tatsuya Nakatani[2] and Hideki Wanibuchi[1,3]

[1]Department of Pathology, [2]Department of Urology, Osaka City University Graduate School of Medicine, Osaka, Japan

(Received January 31, 2012/Revised March 26, 2012/Accepted April 4, 2012/Accepted manuscript online April 12, 2012/Article first published online June 4, 2012)

The object of the present study was to identify markers for predicting urinary bladder cancer progression by comparative proteome analysis of bladder cancers and paired normal mucosas. We found that DDX39 was overexpressed in four of six bladder cancers examined compared with respective control tissues. Immunohistochemical analysis using 303 bladder cancer specimens revealed that DDX39 was inversely correlated to pT stage and histological grade progression. The incidence of DDX39^{high} tumors (positive cells ≥50%) was 68.6%, 43.5%, 20.0%, and 5.3% in pTa, pT1, pTis, and ≥pT2 tumors, respectively, and 65.2%, 60.7%, and 19.6% in G1, G2, and G3 tumors, respectively. The incidence of DDX39^{high} tumors was significantly lower in pT1 and ≥pT2 compared to pTa tumors, and also significantly lower in G3 compared to G1 and G2 tumors. Follow-up analysis (n = 105) revealed that DDX39^{low} tumors (positive cells <50%) were associated with disease progression (hazard ratio 7.485; P = 0.0083). Furthermore, DDX39-knockdown bladder cancer cells increased their invasion ability compared to negative control cells. These results suggest that DDX39 is a suppressor of invasion and loss of its function predicts disease progression in bladder cancers. (*Cancer Sci* 2012; 103: 1363–1369)

Urinary bladder cancers account for approximately 54% of cancers of the urinary system (kidney, renal pelvis, ureters, bladder, and urethra).[1] Approximately 90% of all bladder cancers are urothelial carcinomas.[2] At initial presentation, up to 70% of tumors are non-muscle-invasive, whereas the remainder present with muscle-invasive disease.[3] The treatment for bladder cancer completely differs depending on stage. Generally, non-muscle-invasive bladder cancer (NMIBC) requires transurethral resection of the bladder tumor (TUR-Bt), whereas most muscle-invasive bladder cancer (MIBC) requires radical cystectomy with or without systemic chemotherapy. However, the prognosis for advanced bladder cancer is poor despite recent therapeutic advances.[4] To date, pathological data, including grade, stage, and associated carcinoma *in situ* (CIS) at initial presentation, have provided some insight into predicting the likelihood of progression of bladder cancer.[5,6] Nevertheless, the ability to predict progression remains a challenge as bladder tumors with the same stage and grade have a heterogeneous clinical outcome. This might be due to differences in molecular expression profile. Furthermore, understanding the molecular biology of bladder cancer may provide new therapeutic strategies.

Various molecules have been reported to be associated with the progression of bladder cancer. Tumor suppressor genes, such as *p53*, have been widely studied in bladder cancer, however, its predictive value in assessing the risk of disease progression remains controversial.[7–9] Ki-67 has some prognostic value for predicting recurrence, however, further studies are necessary and the marker is not yet clinically applicable.[10,11] Recently, proteome analysis has been widely used in the study of urine from bladder cancer patients to identify biomarkers.[12] Various urinary markers for the early detection of bladder cancer have been reported, but reliable urinary markers capable of predicting cancer progression have not been established. This is partly due to the fact that some of them are not expressed in bladder tissues.[13] Therefore, investigation of protein expression profiling in bladder cancer tissues will facilitate not only understanding the behavior of cancer cells but also identification of markers of progression of bladder cancer.

The purpose of the present study is to identify markers of bladder cancer progression by comparative proteome analyses of human bladder cancer and paired normal tissues using QSTAR Elite liquid chromatography with tandem mass spectrometry and iTRAQ technology.

Materials and Methods

Patients. Six pairs of snap-frozen bladder urothelial carcinomas and normal mucosa from cystectomy specimens were used for proteome analyses. The clinicopathological characteristics of the bladder carcinomas was as follows: case 1 was pT1, G3; case 2 was pTa, G3; case 3 was pT1, G3; case 4 was pT1, G2; case 5 was pT2a, G3; and case 6 was pT3, G3. Four cases (1–4) were NMIBCs and the remaining cases (5 and 6) were MIBCs. Immunohistochemical analysis was carried out on samples from 303 patients who were treated for bladder cancer by TUR-Bt or cystectomy at Osaka City University Hospital (Osaka, Japan) between 2000 and 2009. There were 248 men (81.8%) and 55 women (18.2%), and the median age was 68 years (range, 33–90 years). Among these patients, those with CIS and those who were incompletely resected and lost to follow-up were excluded from the study. The patients who were treated by total cystectomy were also excluded, because almost all of these patients had already progressed to muscle-invasive disease. One hundred and five TUR-Bt cases (between 2004 and 2007), for which full clinical data were available, were used for follow-up analysis. Pathologic staging was carried out according to the 2002 TNM classification system,[14] and grading was done according to the 1973 World Health Organization criteria for continuity of the study, as many samples were obtained before the 2004 criteria were published. The Institutional Review Board at Osaka City University Graduate School of Medicine approved the use of the specimens and clinical data in accordance with the Declaration of Helsinki and guidelines of Osaka City University Graduate School of Medicine.

Proteome analyses. Pathologic diagnoses of the six urothelial cancers and paired control tissues were confirmed before proteome analyses. Reagents, except for those specifically noted, were obtained from AB Sciex (Foster City, CA, USA). The

[3]To whom correspondence should be addressed.
E-mail: wani@med.osaka-cu.ac.jp

doi: 10.1111/j.1349-7006.2012.02298.x

specimens were homogenized and dissolved in 300 μL T-PER Tissue Protein Extraction Reagent (Thermo Scientific, Rockford, IL, USA) with protease inhibitor. After brief ultrasonication, insoluble material was removed by centrifugation at 13 000*g* for 15 min at 4°C. Protein concentration of the supernatant was measured by the BCA Protein Assay Kit (Pierce, Rockford, IL, USA). Protein reduction, alkylation, and subsequent peptide labeling were carried out using iTRAQ Reagent Multiplex Kit (AB Sciex, Foster City, CA, USA). Samples (100 μg of each) were resuspended in 20 μL of dissolution buffer (0.5 M triethylammonium bicarbonate at pH 8.5). One microliter of denaturant (2% SDS) and 2 μL reducing reagent (50 nM tris-(2-carboxyethyl) phosphine) were added and incubated at 60°C for 60 min. Free sulfhydryl groups of cysteines were blocked with 1 μL cysteine blocking reagent (20 mM methyl methanethiosulfonate) and incubated at room temperature for 10 min. Trypsin solution (10 μg) was added to each sample and incubated at 37°C overnight. Tryptic peptides of each sample were labeled with iTRAQ tags by incubation at room temperature for 1 h. Each of the samples was then mixed in one tube and fractionated by six concentrations of KCl solutions (10, 50, 70, 100, 200, and 350 mM) using ICAT cation exchange cartridge. Supernatant was evaporated in a vacuum centrifuge. Peptides of each fraction were resuspended into 2 mL of 2% acetonitrile and desalted using Sep-Pak Light C18 cartridge (Waters, Milford, MA, USA). The supernatant was dissolved in 20 μL of 0.1% formic acid.

Proteome analysis was carried out with a DiNa-AI nano system (KYA Technologies, Tokyo, Japan) coupled to a QSTAR EliteHybrid mass spectrometer through a NanoSpray ion source. Protein identification was done with ProteinPilot 2.0 software (AB Sciex).

Immunohistochemical analysis of DDX39. Formalin-fixed, paraffin-embedded tissues of 303 patients with bladder cancer were analyzed by immunohistochemical staining. Sections (3 μm-thick) were cut and deparaffinized in xylene and rehydrated in alcohols and distilled water. Endogenous peroxidase was blocked with 3% hydrogen peroxide in distilled water for 5 min, followed by washing in PBS three times. Sections were then incubated with 1.5% goat serum in PBS for 15 min to bind non-specific antigens and then with rabbit polyclonal antibody to DDX39 (ab96621, 1:500; Abcam, Cambridge, MA, USA) at 4°C overnight. This was followed by incubation with biotinylated goat anti-rabbit IgG for 30 min and avidin–biotin peroxidase complex for 30 min at room temperature. Antigen was detected with 3,3-diaminobenzidine and counterstaining with hematoxylin.

Immunohistochemical analysis was carried out by two pathologists who were blinded to the clinical data (S.Y. and H.W.). Immunoreactivity of DDX39 was observed in nuclei of bladder tissues but not in the normal urothelium. Under a microscope at ×200 magnification on six random fields per sample, tissues with $\geq$50% cancer cells immunoreactive for DDX39 were defined as $DDX39^{high}$, and those with <50% cells immunoreactive for DDX39 were defined as $DDX39^{low}$.

Cell lines. Human bladder cancer cell lines T24, TCCSUP, and UMUC3 were purchased from ATCC (Rockville, MD, USA). All cells were maintained as monolayer cultures at 37°C and 5% CO_2. T24 was grown in McCoy's medium and TCCSUP and UMUC were grown in MEM. All media were supplemented with 10% FBS.

Western blot analyses. Whole cell lysates were collected using a cell scraper and resupended in CelLytic MT (Sigma, St Louis, MO, USA) with protease inhibitor. The amount of total protein was determined using a BCA protein assay kit (Pierce). Protein (15 μg of each) was loaded on 10% SDS–polyacrylamide gels. Proteins were transferred to a PVDF membrane and blocked with 5% skimmed milk in TBS buffer containing 0.1% Tween-20. The membrane was probed with primary antibody for DDX39 (ab50697, 1:100; Abcam) or β-actin (ab49900, 1:100 000; Abcam) for 1 h at room temparature. After washing, the membrane was incubated for 1 h at room temperature linked with HRP-conjugated secondary antibody (#sc-2004, 1:10 000; Santa Cruz Biotechnology, Santa Cruz, CA, USA). Immunoreactive bands were detected using the ECL Plus Western blotting system (GE Healthcare, Piscataway, NY, USA) and LAS-3000 image analysis system (Fujifilm, Tokyo, Japan).

Real-time PCR. Total RNA was extracted from cell lines using the RNeasy Mini kit (Qiagen, Tokyo, Japan) according to the manufacturer's instructions. RNA concentration was determined by Nanodrop (Thermo Scientific). RNA (1 μg) was used for cDNA synthesis using Advantage RT-for-PCR kit (Takara Bio, Tokyo, Japan). The real time RT-PCR assay was carried out with the Applied Biosystems 7500 Fast real-time PCR machine (Applied Biosystems, Foster City, CA, USA). Real-time RT-PCR reactions consisted of 10 μL of 2× TaqMan FAST Universal Master Mix (Applied Biosystems), 1 μL of 20× TaqMan Gene Expression Assay (Applied Biosystems), and 1 μg cDNA solution. The assay IDs used for real-time RT-PCR were as follows: DDX39, Hs00271794_m1; and GAPDH, Hs00266705_g1. The thermal cycle program was: 20 s at 95°C followed by 40 cycles of 3 s at 95°C and 30 s at 60°C. The data were then quantified using the comparative C_t method for relative gene expression compared with GAPDH as internal control.

Knockdown of DDX39. DDX39 expression was transiently knocked down using Lipofectamine RNAiMAX (Invitrogen, Carlsbad, CA, USA) according to the manufacturer's instructions. DDX39-specific siRNAs (Silencer Select SiRNA; Cat.# s19917 and s19918) were obtained from Life Technologies (Grand Island, NY, USA). Non-targeting control siRNA (Pre-miR miRNA Precursor Starter Kit, Cat.# AM1540) was obtained from Life Technologies. T24 cells (3×10^5) were transiently transfected with 10 nM s19917, s19918, or control SiRNA in a six-well plate. After 24 h, cells were trypsinized and used in cell proliferation and cell invasion assays.

Cell proliferation assay. T24 cells (1×10^4/well) were seeded in a 96-well plate and transfected with 10 nM DDX39 siRNAs and control siRNA. After 24 h, cell proliferation was measured using a Cell Counting Kit-8 (Dojindo Laboratories, Tokyo, Japan) according to the manufacturer's instructions. The number of cells was measured with a microplate reader (Bio-Rad, Tokyo, Japan) at 450 nm.

Cell invasion assay. Invasion was assessed in a QCM cell invasion assay (Millipore, Billerica, MA, USA), according to the manufacturer's protocol. Briefly, transfectants (2×10^5 cells) were seeded in the upper chamber, whereas the lower chamber was loaded with medium containing 10% FBS. After a 24-h incubation at 37°C, the cells that invaded the reverse side of the insert were dislodged by incubating the insert in 225 μL cell detachment buffer for 30 min at room temparature. Lysis buffer and CyQuant GR Dye mixture (75 μL each) were added in detachment buffer and the plate was incubated for 15 min in the dark. Then 200 μL of the mixture was transferred to a 96-well plate and measured with a fluorescence plate reader at 480/520 nm.

Statistical analysis. Statistical analyses were carried out with SPSS version 19 (IBM, Armonk, NY, USA). Fisher's exact test was used to evaluate the differences in incidence of DDX39 expression patterns among clinical and pathological parameters. The progression-free survival was defined as the time between the date of surgery and the last date of follow-up or date of progression in pT status. The curves were done using the Kaplan–Meier method with the log–rank test to assess statistical significance. Cox proportional hazards analysis was used to determine the relative contribution of various factors to the risk of progression. $P < 0.05$ was considered statistically significant.

doi: 10.1111/j.1349-7006.2012.02298.x

Results

Proteome analysis. We identified 493 proteins by proteomic analysis of six sample pairs. Overexpressed proteins were selected according to the criteria that the fold difference had to be >1.2.[15] Fifteen proteins were overexpressed in cancer tissues compared to adjacent normal tissues in four or more of six sample pairs (Table 1). To validate the results of the proteome analysis, immunohistochemical staining of the above proteins in 303 bladder specimens was carried out, except for those that have already been evaluated in bladder cancers (Ezrin, nucleophosmin, prothymosin alpha, S100 calcium binding protein A11, and S100 calcium binding protein P).[16–19] Actin-related protein 3 homolog B was not evaluated as no commercial antibody was available.

Results of immunohistochemistry analyses of DDX39, B-cell receptor-associated protein 31, chaperonin containing TCP1, FK506 binding protein 4, isocitrate dehydrogenase 1, keratin 19, myosin heavy chain 9 non-muscle, prolyl 4-hydroxylase beta polypeptide, and Y box binding protein 1 revealed that DDX39, but not the other proteins, was expressed in a different manner according to cancer stage and grade as described below, although all of them showed high expression levels in cancer compared to control tissues.

Expression of DDX39 in bladder cancers. The clinicopathological parameters of the patients whose tissues were used for immunohistochemical analysis are summarized in Table 2. As shown in Figure 1, nuclear staining of DDX39 was not observed in normal urothelium (Fig. 1D). Unexpectedly, expression levels of DDX39 were apparently lower in MIBCs when compared with NMIBCs. As summarized in Table 2, the incidence of $DDX39^{low}$ cancers was 31%, 56%, 80%, and 95% in pTa, pT1, pTis, and ≥pT2 tumors, respectively. The incidence of $DDX39^{low}$ cancers was significantly higher in ≥pT2 compared to pT1 and pTa cancers, and also significantly higher in pT1 when compared to pTa. Furthermore, the incidence of $DDX39^{low}$ cancers was 35%, 39%, and 80% in G1, G2, and G3 tumors, respectively, and significantly higher in G3 when compared to G1 and G2 tumors.

Follow-up of patient outcomes and survival analysis. Correlation analysis of DDX39 expression level and recurrence/progression-free survival in 105 bladder cancer patients who were treated by TUR-Bt revealed that $DDX39^{low}$ cancers showed rapid disease progression ($P = 0.0083$; Fig. 2A). Moreover, rapid disease progression was also evident in $DDX39^{low}$ cancers when the 78 pTa cancers were analyzed from the above cases ($P = 0.0027$; Fig. 2B). No association was found with recurrence-free survival in either of the analyses (data not shown).

Univariate and multivariate analyses. Univariate and multivariate analyses of clinicopathological parameters and progression-free survival revealed that low expression of DDX39 was an independent risk factor for progression (Tables 3,4).

Expression levels of DDX39 and invasion ability of bladder cancer cells. The mRNA expression levels of DDX39 were analyzed by real-time PCR in T24, TCCSUP, and UMUC3 cells. T24 cells showed the highest expression level of DDX39 (Fig. 3A) but the lowest invasion ability among the three bladder cancer cell lines (Fig. 3B). As T24 showed an inverse relationship between the expression level of DDX39 and its invasion ability, similar to that observed in the bladder cancer

Table 2. Clinicopathological characteristics of patients ($n = 303$), stages and grades of bladder cancer, and DDX39 expression

Parameters	DDX39 high expression tumors (%)	P-value
Age (68 ± 10.5 years)		
<65 years (n = 116)	52 (44.8)	NS
≥65 years (n = 187)	103 (55.1)	
Gender		
Male (n = 248, 81.8%)	127 (51.2)	NS
Female (n = 55, 18.2%)	28 (50.1)	
Stage		
pTa (n = 169, 55.7%)	116 (68.6)	
pT1 (n = 62, 20.5%)	27 (43.5)	0.0005*
≥pT2 (n = 57, 18.8%)	3 (5.3)	<0.0001* <0.0001†
pTis (n = 15, 5.0%)	3 (20.0)	0.0003*
Grade		
G1 (n = 66, 21.8%)	43 (65.2)	
G2 (n = 145, 47.9%)	88 (60.7)	
G3 (n = 92, 30.4%)	18 (19.6)	<0.0001**,††

*Statistically significant from pTa. **Statistically significant from G1. †Statistically significant from pT1. ††Statistically significant from G2. NS, not significant.

Table 1. Upregulated proteins in cancer tissues using liquid chromatography with tandem mass spectrometry

Symbol	Case						Full name	Location
	1	2	3	4	5	6		
ACTR3B	4.200	2.359	ND	1.718	1.818	16.933	Actin-related protein 3 homolog B (yeast)	Unknown
BCAP31	2.797	2.186	ND	1.38	2.704	ND	B-cell receptor-associated protein 31	Cytoplasm
CCT4	4.008	1.561	1.650	1.296	ND	7.610	Chaperonin containing TCP1, subunit 4 (delta)	Cytoplasm
DDX39	4.685	1.858	2.116	ND	1.900	ND	DEAD (Asp-Glu-Ala-Asp) box polypeptide 39	Nucleus
EZR	4.961	2.315	1.536	1.776	3.113	4.704	Ezrin	Plasma membrane
FKBP4	19.763	3.820	2.308	ND	3.500	ND	FK506 binding protein 4	Nucleus
IDH1	4.618	3.137	1.278	1.580	2.662	ND	Isocitrate dehydrogenase 1 (NADP+), soluble	Cytoplasm
KRT19	3.101	4.917	ND	1.437	5.312	4.614	Keratin 19	Cytoplasm
MYH9	2.918	2.888	1.413	1.473	2.438	6.401	Myosin, heavy chain 9, non-muscle	Cytoplasm
NPM1	1.529	1.240	ND	ND	1.684	11.318	Nucleophosmin (nucleolar phosphoprotein B23, numatrin)	Nucleus
P4HB	3.690	1.431	1.378	ND	2.286	10.049	Prolyl 4-hydroxylase, beta polypeptide	Cytoplasm
PTMA	3.477	1.165	1.860	ND	2.102	3.062	Prothymosin, alpha	Nucleus
S100A11	8.414	1.991	1.311	1.512	5.261	9.114	S100 calcium binding protein A11	Cytoplasm
S100P	6.842	5.731	ND	2.128	8.834	3.450	S100 calcium binding protein P	Cytoplasm
YBX1	2.978	1.711	1.644	ND	1.912	ND	Y box binding protein 1	Nucleus

The numbers listed under cases 1–6 indicate the fold change of the protein expression level of cancer tissue compared to normal tissue in each case. ND, not detectable.

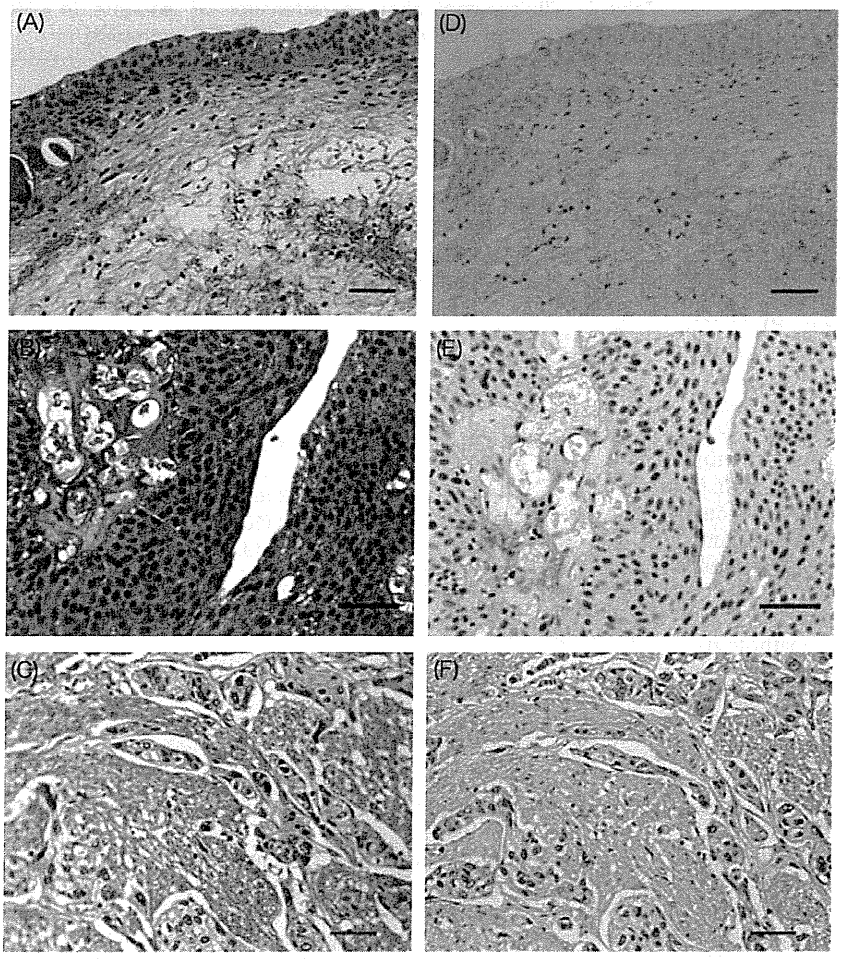

Fig. 1. Hematoxylin–eosin staining (A–C) and immunohistochemical staining (D–F) for DDX39 of normal urothelium and bladder cancers. (A,D) Normal bladder urothelium; (B,E) DDX39^{high} (positive cells ≥50%) pTa cancer; (C,F) DDX39^{low} (positive cells <50%) pT2 cancer. Bar = 50 μm.

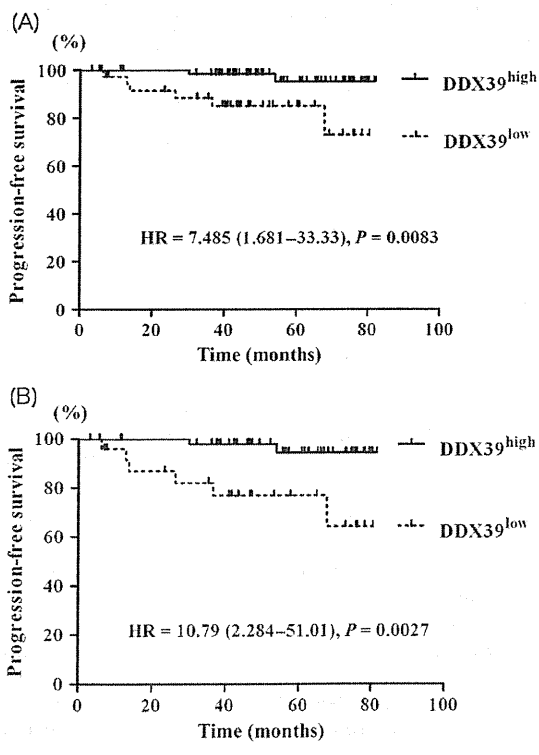

Fig. 2. DDX39^{low} cancers (positive cells <50%) showed rapid disease progression in pTa and pT1 cancers (A) (n = 105) and pTa cancers (B) (n = 78). HR, hazard ratio.

specimens analyzed above, we used T24 cells to investigate the effects of DDX39 knockdown on invasion ability.

Effect of DDX39 knockdown on cell proliferation and invasion ability of T24 cells. Western blot analysis showed a remarkable reduction in protein level of DDX39 in T24 cells transfected with si-DDX39 A (s19917) and B (s19918) compared with the negative control (Fig. 4A). Furthermore, real-time PCR analysis showed that si-DDX39 A and B reduced DDX39 mRNA expression levels by 71% and 74%, respectively, compared with the negative control (Fig. 4B). Although knockdown of DDX39 by si-DDX39 A and B had no effect on cell proliferation (Fig. 5A), T24 cells transfected with si-DDX39 A and si-DDX39 B showed 2.36- and 2.65-fold higher invasion activity, respectively, compared to the negative control (Fig. 5B).

Discussion

The results of the present study indicated that the expression level of DDX39 is significantly lower in MIBCs compared to NMIBCs. We also found that the DDX39 expression level was significantly correlated with pT stage and grade, and DDX39^{low} cancers showed rapid disease progression. Furthermore, knockdown of DDX39 increased the invasion ability of bladder cancer cells. These findings indicated that DDX39 is a suppressor of invasion and loss of its function predicts disease progression in bladder cancers. To the best of our knowledge, the present study showed for the first time the relationship between DDX39 expression and cancer cell invasion.

A member of the RNA helicases, DDX39 is involved in pre-mRNA splicing.[20] RNA helicase is thought to be required

doi: 10.1111/j.1349-7006.2012.02298.x

Table 3. Univariate analyses of various clinicopathological parameters in relation to progression-free survival of patients with bladder cancer

Patients	Progression-free survival		
Parameters	No. cases (%)	No. events	P-value†
Age (years)			
<65	46 (44)	2	0.2971
≥65	59 (56)	6	
Gender			
Male	84 (80)	6	0.6708
Female	21 (20)	2	
Stage			
pTa	78 (74)	8	0.1050
pT1	27 (26)	0	
Grade			
G1 + G2	90 (86)	6	0.3695
G3	15 (14)	2	
Concominant CIS			
No	98 (93)	7	0.4638
Yes	7 (7)	1	
No. tumors			
Single	76 (72)	4	0.1624
Multiple (2–7)	29 (28)	4	
Tumor size			
<3 cm	101 (96)	8	0.6123
≥3 cm	4 (4)	0	
Tumor status			
Primary	76 (72)	4	0.1830
Recurrent	29 (28)	4	
DDX39 expression			
Low (positive cells <50%)	39 (37)	6	0.0083
High (positive cells ≥ 50%)	66 (63)	2	

†Log–rank test. CIS, carcinoma in situ.

Table 4. Multivariate analyses for progression free survival

Variables	Progression-free survival	
	OR (95% CI)	P-value
Grade		
G1 + G2	1	–
G3	1.084 (0.140–8.420)	0.938
Carcinoma in situ		
–	1	–
+	2.369 (0.178–31.484)	0.514
No. tumors		
Single	1	–
Multiple	2.532 (0.570–11.250)	0.222
Prior recurrence rate		
Primary	1	–
Recurrence	1.035 (0.337–3.176)	0.952
DDX39 expression		
High	1	–
Low	7.171 (1.284–40.063)	0.025

–, normalized.

for the export of mRNA out of the nucleus, transcription, splicing, and transport of mRNA.[21] Although several other RNA helicases were reported to be dysregulated in cancer, and loss of normal function of RNA helicase could result in abnormal RNA processing,[22] little is known about the exact roles of RNA helicases in carcinogenesis. Sugiura *et al.*[23] reported that DDX39 was upregulated in lung squamous cell

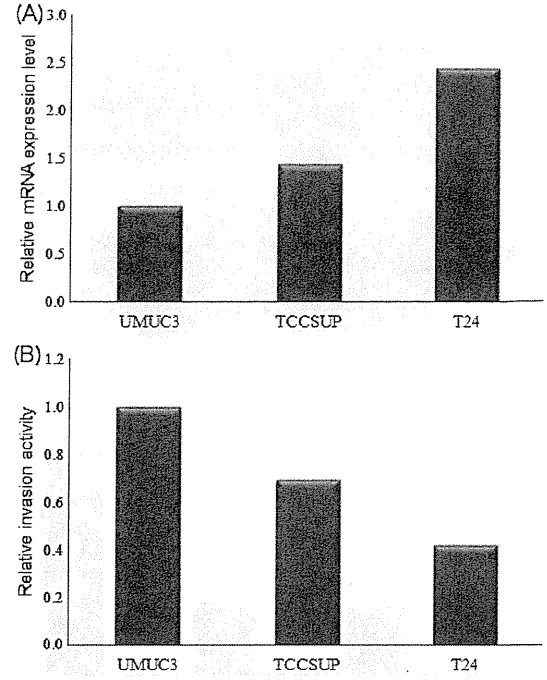

Fig. 3. mRNA expression of DDX39 (A) and cell invasion ability (B) of UMUC3, TCCSUP, and T24 bladder cancer cells. The DDX39 expression level was highest, but the invasion ability was lowest, in T24 cells compared to the other two cell lines.

cancer and promoted cancer cell growth. However, we found that DDX39 inhibits the invasion, but had no effect on proliferation, of bladder cancer cells. Although the exact role of DDX39 in bladder carcinogenesis is not known, the fact that the expression level of DDX39 is significantly higher in NMIBCs compared to MIBCs, and that DDX39 has no effect on cell proliferation and is not expressed in normal bladder mucosa, suggested that DDX39 in NMIBCs may exert a protective role against bladder cancer invasion. Furthermore, based on the finding that DDX39^{low} pTa cancers showed rapid disease progression, DDX39 might serve as a marker for NMIBCs that are likely to progress; those showing low levels of DDX39 may require more intensive therapy and closer follow-up. Further study is needed to evaluate the underlying mechanisms by which DDX39 inhibits the invasion of bladder cancer.

Matrix metalloproteinase 2 and 9 and E-cadherin were reported to be associated with bladder cancer invasion.[24,25] In the present study, the mRNA expression level of MMP2, MMP9, and E-cadherin did not change significantly by DDX39 knockdown (data not shown). These results suggested that DDX39 inhibited invasion by mechanisms independent of these proteins.

Recurrence and progression are the main problems for NMIBCs, but few reports are available identifying molecules that could predict progression. The European Association of Urology (EAU) guideline on non-muscle-invasive urothelial carcinoma of the bladder has already proven to be useful to predict recurrence and progression,[26] but its classification system is quite complicated to apply clinically. In addition, stratification based on the EAU guidelines for recurrence is not fully applicable to Japanese patients with bladder cancers.[27] In the present study, cancer stage, histological grade, concomitant CIS, number of tumors, size of tumors, and prior recurrence rate could not predict cancer progression. This might be partially due to the sample size of our patients' dataset. But the results of the present study showed that only